$H \rightarrow WW^*$ in ATLAS

Young Scientist Forum

Pere Rados

The University of Melbourne, CoEPP

31/8/2016

On behalf of the ATLAS Collaboration

Higgs production and decay

Phys. Rev. Lett. 114, 191803

- Higgs boson property measurements are an essential test of SM validity
- Search for evidence of more rare production modes
- In parallel search for additional high mass states

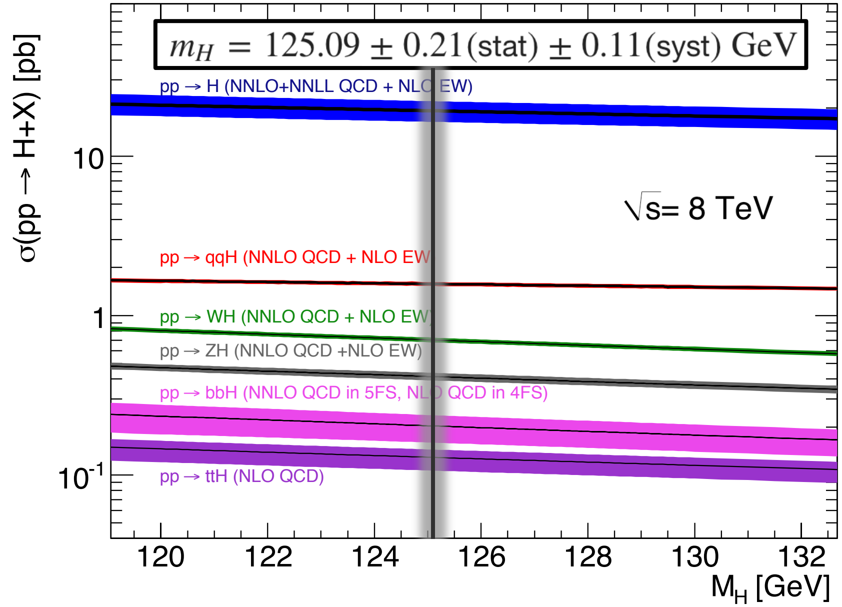

ggF 87%

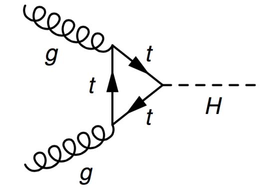

VBF 7%

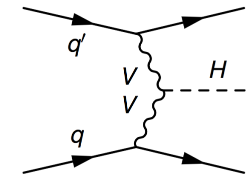

***WH/ZH* 5%**

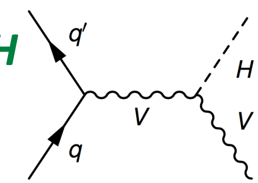

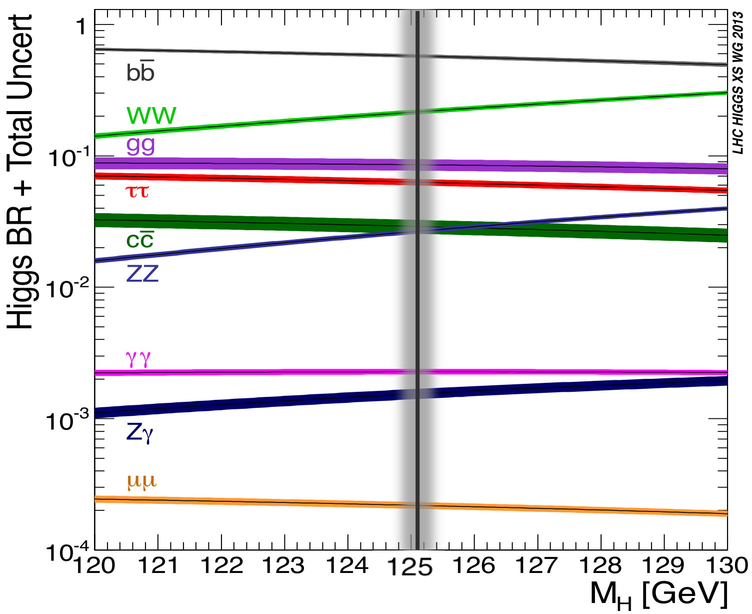

H→WW* **22%**

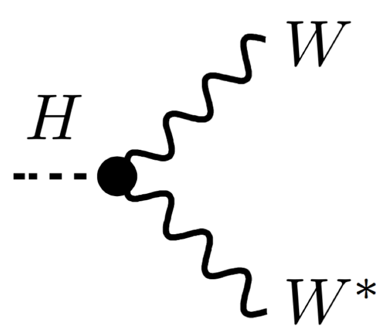

- WW^* decay channel plays an important role:
  - Large branching ratio
  - Good S/B in the di-lepton final state $H \to WW^* \to l\nu l\nu$

$H \rightarrow WW^*$ Signature

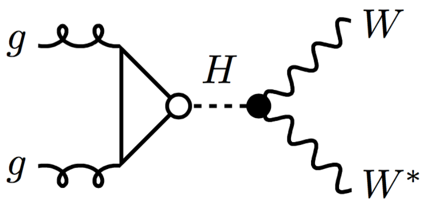

ggF channel
- 2 leptons
- Large E_T^{miss} (2ν)
- Low jet multiplicity

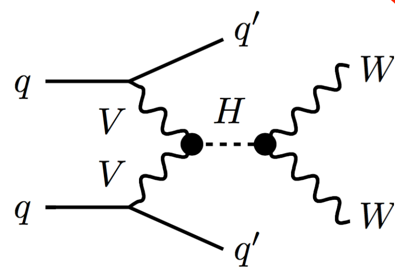

VBF channel
- 2 leptons
- Large E_T^{miss} (2ν)
- 2 forward jets

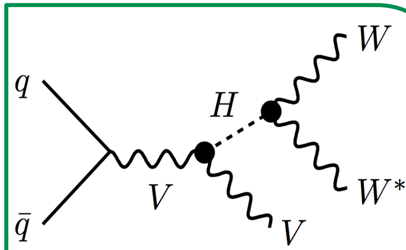

WH/ZH channels
- 3/4 leptons
- Large E_T^{miss} (3/2ν)
- Low jet multiplicity

- **All channels**: 2 leptons from Higgs tend to have small angular separation

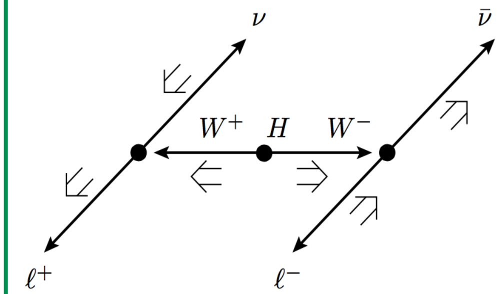

- *H→WW*→lνlν* final state cannot be fully reconstructed due to presence of neutrinos
  - The **transverse mass (m_T)** can be calculated without the unknown longitudinal neutrino momenta

$$m_{\mathrm{T}} = \sqrt{(E_{\mathrm{T}}^{\ell\ell} + p_{\mathrm{T}}^{\nu\nu})^2 - |\boldsymbol{p}_{\mathrm{T}}^{\ell\ell} + \boldsymbol{p}_{\mathrm{T}}^{\nu\nu}|^2}$$

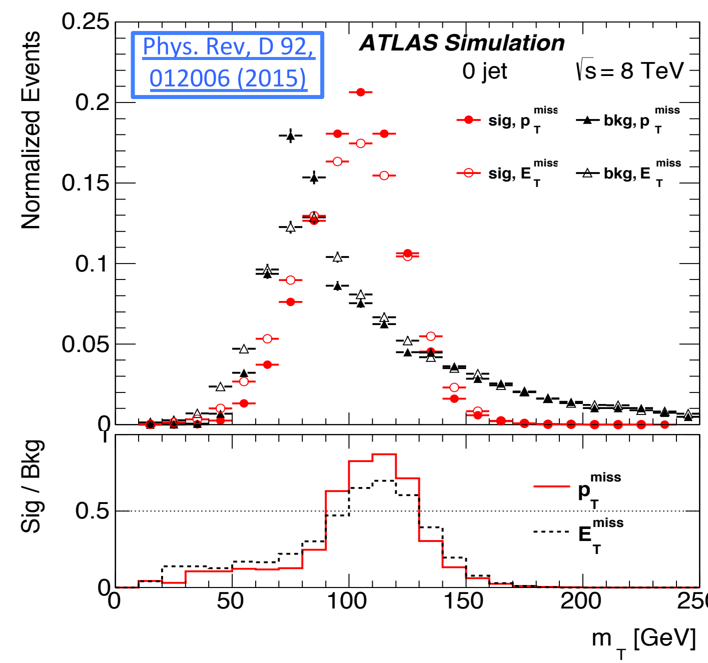

ggF/VBF analysis strategy

[Phys. Rev, D 92, 012006 (2015)]

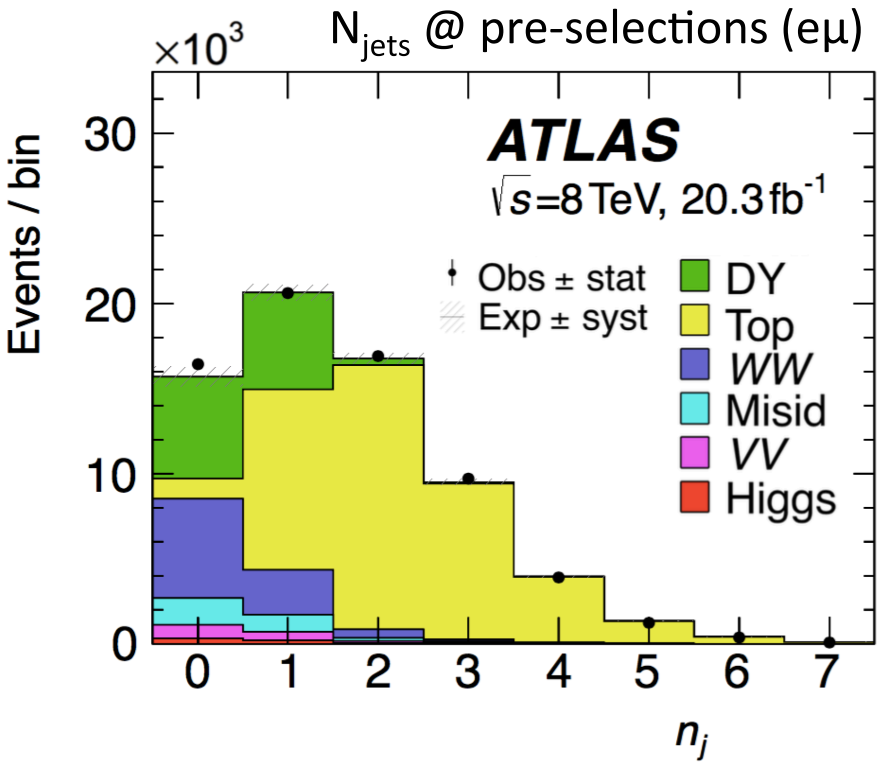

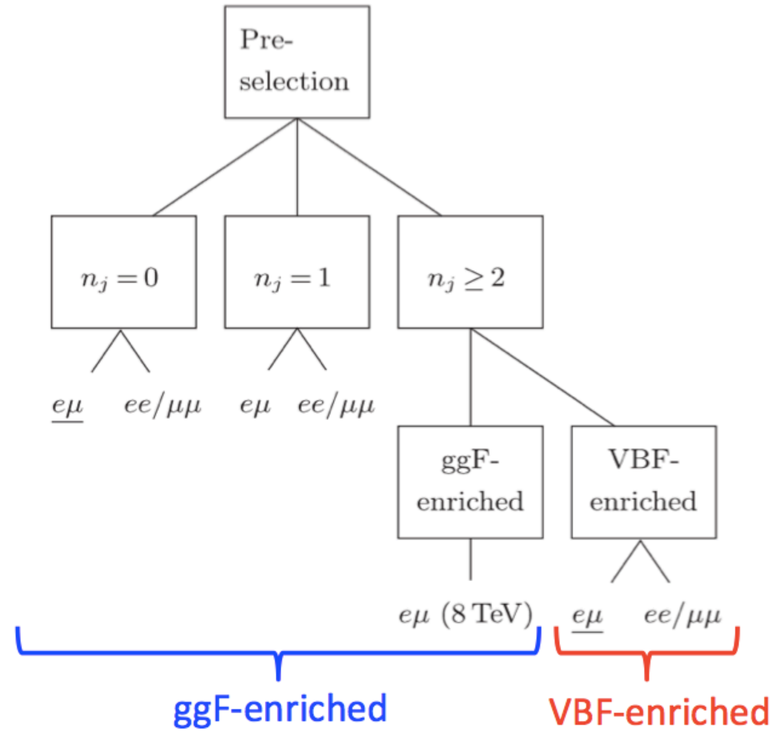

- Categorize events according to jet multiplicity and lepton flavour
  - **0-jet** and **1-jet** are ggF dominated, while **≥2-jet** is VBF dominated
  - ***eμ*** channel is cleanest and most sensitive, while ***ee*** and ***μμ*** have large *Z*/Drell-Yan background
- Reduce backgrounds with selections optimized for each category
- **ggF-enriched** analysis is cut-based, while **VBF-enriched** is BDT-based

ggF/VBF Backgrounds

[Phys. Rev, D 92, 012006 (2015)]

WW
- Dominant background in 0 and 1 jet categories
- Almost irreducible (larger $\Delta\phi_{ll}$ then signal process)
- m_{ll} used to define CRs for both 0 and 1 jet

Top
- Large contribution, especially in $\geq$ 2 jet categories
- Entering via unidentified b-quark
- Extrapolated using several CRs with $N_{b\text{-jet}} \geq 1$

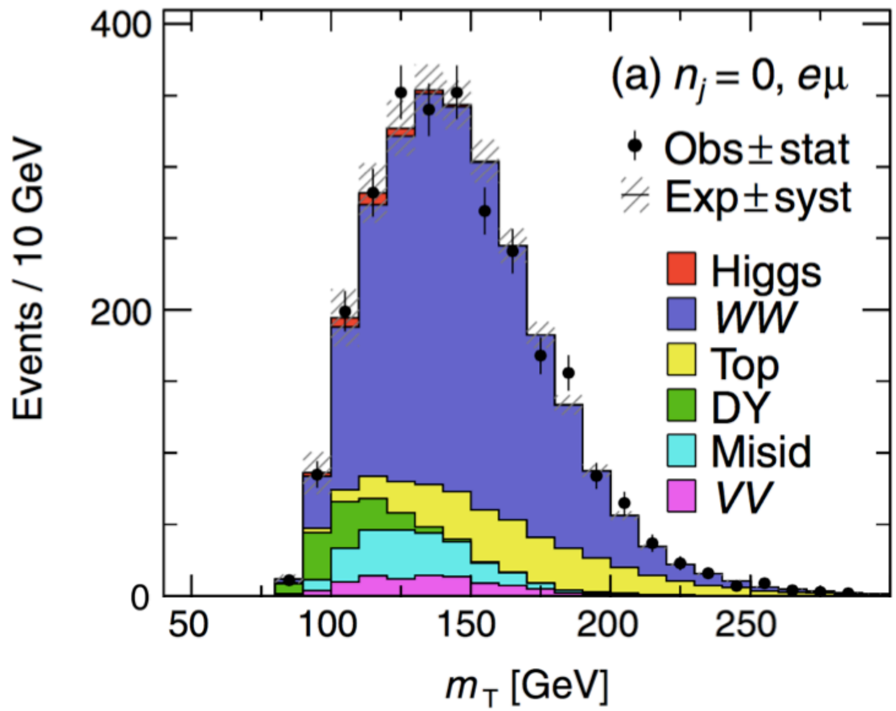

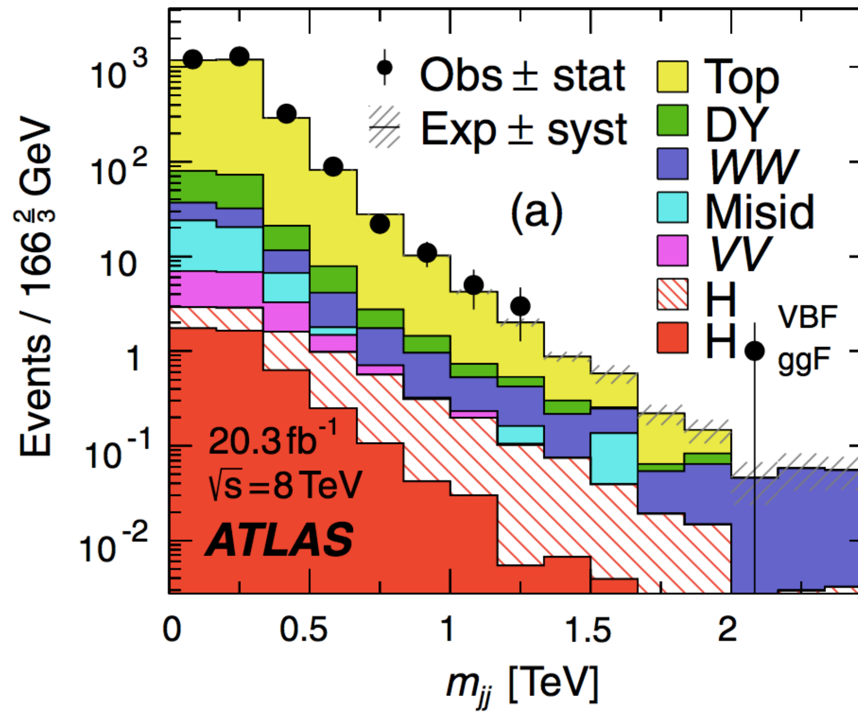

W+jets and multi-jet
- Estimated via a "fake factor" method
- Fake factors are estimated primarily from a *Z*+jets data sample

Z/Drell-Yan
- *Z*/DY→ττ estimated using CRs
- *Z*/DY→*ee*/*μμ* estimated via data driven methods (Pacman, ABCD)

Other Diboson
- *Wγ*, *Wγ**, *WZ* and *ZZ*
- Same-sign CR used for eμ
- Several validation regions

ggF/VBF Signal Strength

Phys. Rev, D 92, 012006 (2015)

JHEP 08 (2015) 137

ggF signal region

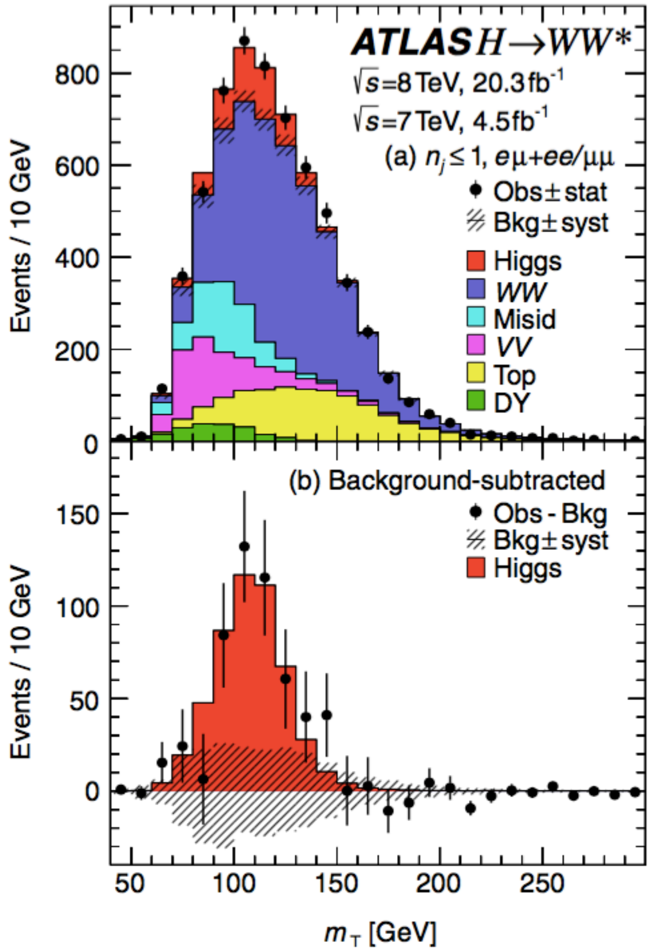

VBF signal region

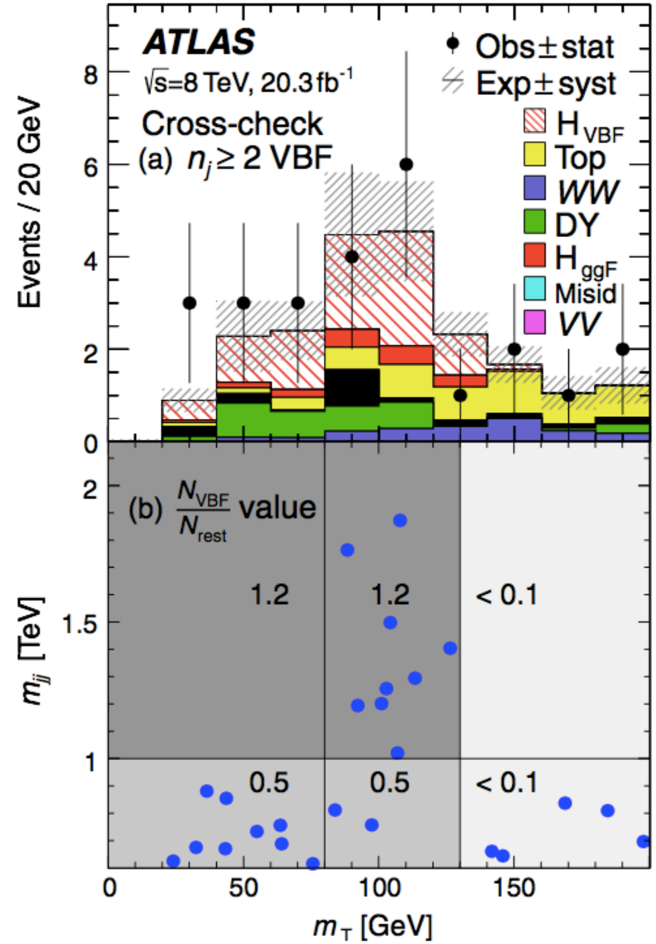

$$\mu_{ggF} = 0.98\ ^{+0.29}_{-0.26}$$

4.2σ evidence for ggF production

(4.4σ expected)

$$\mu_{VBF} = 1.28\ ^{+0.55}_{-0.47}$$

3.2σ evidence for VBF production

(2.6σ expected)

$$\sigma^{7\ \mathrm{TeV}}_{\mathrm{ggF}} \cdot \mathcal{B}_{H\to WW^*} = 2.0\ ^{+2.1}_{-2.0}\ \mathrm{pb}$$

(3.3 ± 0.4 pb predicted)

$$\sigma^{8\ \mathrm{TeV}}_{\mathrm{ggF}} \cdot \mathcal{B}_{H\to WW^*} = 4.6\ ^{+1.2}_{-1.1}\ \mathrm{pb}$$

(4.2 ± 0.5 pb predicted)

$$\sigma^{8\ \mathrm{TeV}}_{\mathrm{VBF}} \cdot \mathcal{B}_{H\to WW^*} = 0.51\ ^{+0.22}_{-0.17}\ \mathrm{pb}$$

(0.35 ± 0.02 pb predicted)

VH Signal Strength

JHEP 08 (2015) 137

WH→ 3 leptons channel

- Major backgrounds are $WZ/W\gamma^*$, ZZ^*, top and *VVV*
- 6 CRs to address bkg normalization
- Analysis split into two regions:
  - Z-depleted (ΔR_{ll} shape analysis)
  - Z-enriched (BDT shape analysis)

Z-depleted SR (0 SFOS)

ΔR_{ll} of Higgs candidate leptons

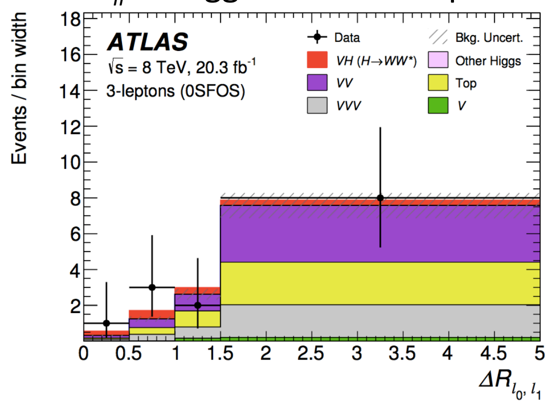

Z-enriched SR (1 SFOS)

BDT score

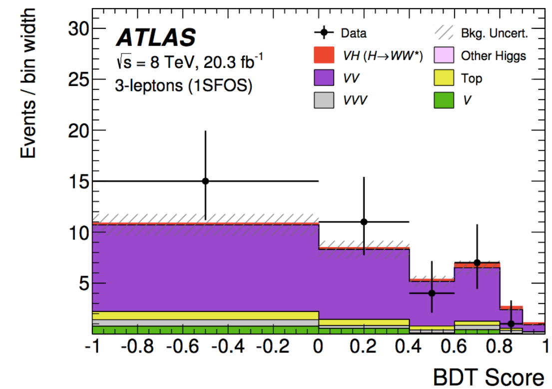

ZH→ 4 leptons channel

- ZZ^* is the major background
- CR used to address ZZ^* normalization
- Analysis split into two regions:
  - 1 SFOS (cut-and-count analysis)
  - 2 SFOS (cut-and-count analysis)

1 SFOS SR

$\Delta\phi_{ll}$ of Higgs candidate leptons

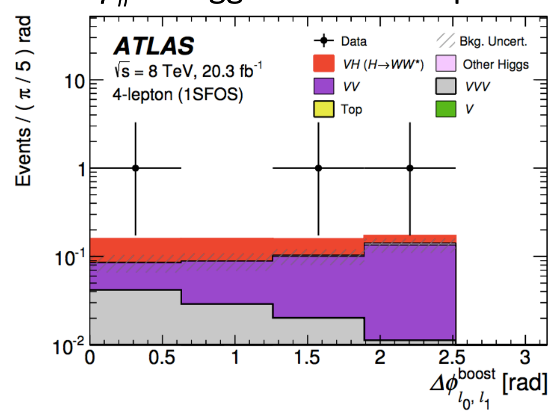

2 SFOS SR

$\Delta\phi_{ll}$ of Higgs candidate leptons

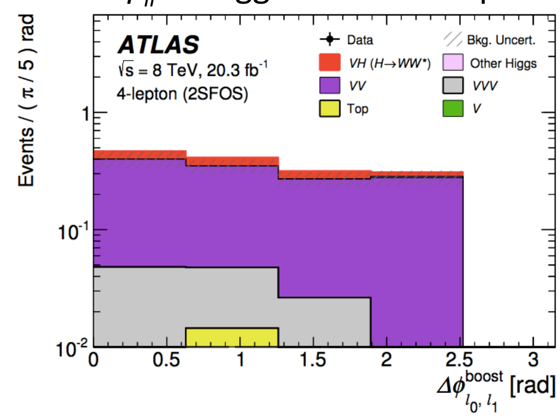

Combining all *VH* channels (including also DFOS + SS di-lepton channels):
Significance of *VH* production is 2.5σ (0.93σ expected)

$$\mu_{VH} = 3.0 \begin{array}{l} +1.6 \\ -1.3 \end{array}$$

Combined Results

JHEP 08 (2015) 137

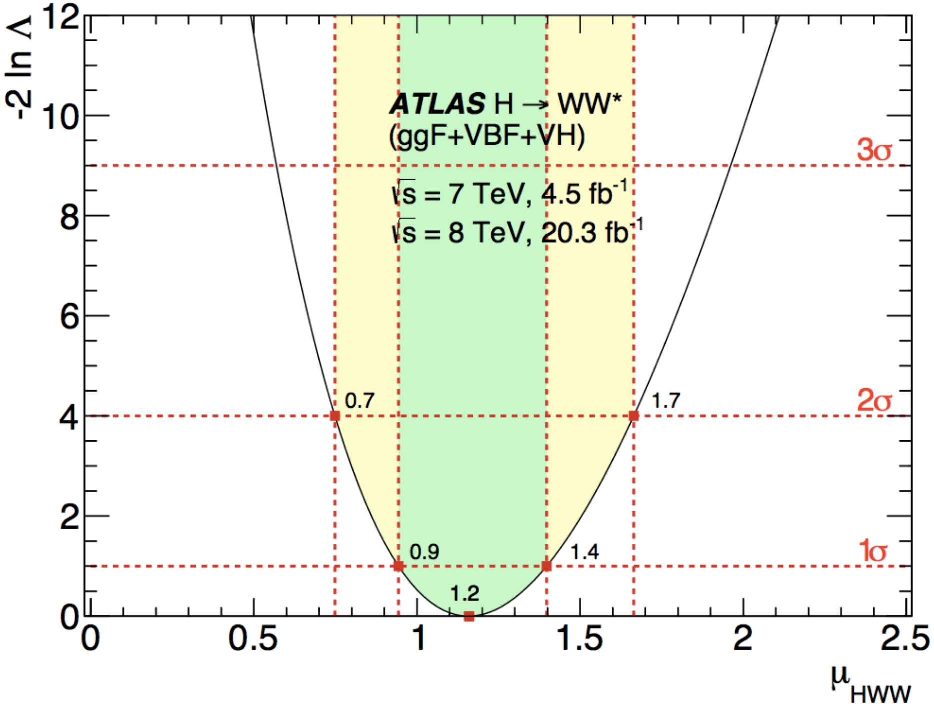

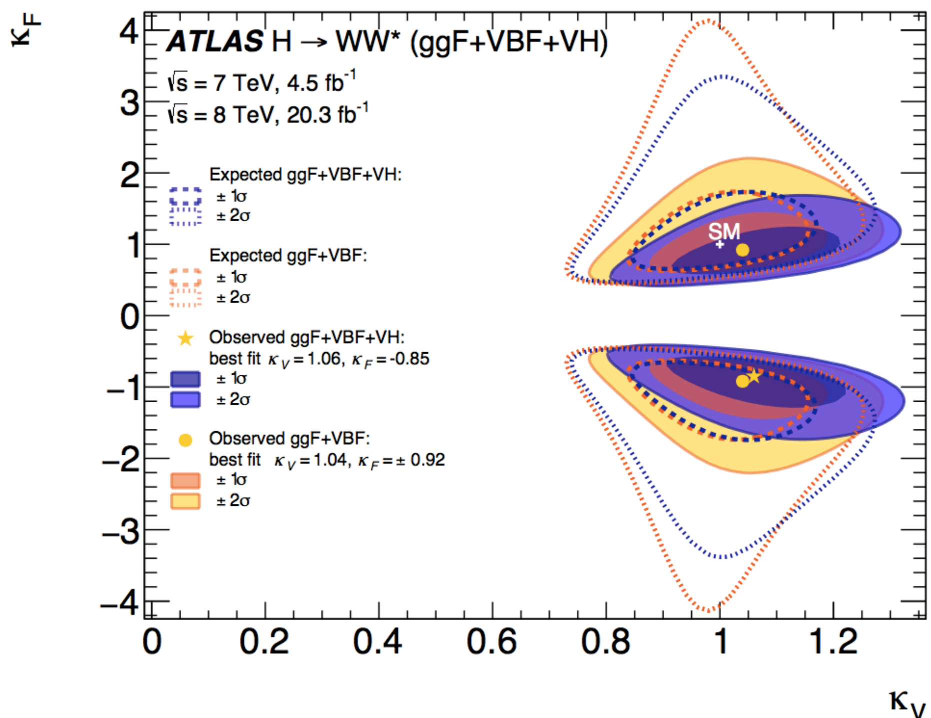

Signal strength for ggF+VBF+*VH*:

$$\mu = 1.16^{+0.16}_{-0.15}(\text{stat.})^{+0.18}_{-0.15}(\text{sys.})$$

Vector boson and fermion couplings:

$$|\kappa_V| = 1.06^{+0.10}_{-0.10} \quad |\kappa_F| = 0.85^{+0.26}_{-0.20}$$

6.5σ significance for *H→WW** (5.9σ expected)

Not shown here are the run-1 spin/CP inputs (Eur. Phys. J. C (2015)) and differential fiducial cross-section measurements (arXiv:1604.02997). More details on these can be found in the backup.

High Mass $H \rightarrow WW^*$ Search

ATLAS-CONF-2016-074

- Motivation: search for a potential extension of the SM with an extended Higgs Sector
- Signal scenarios:
  - "NWA" : SM-like Higgs with narrow width (4 MeV)
  - "LWA" : with large width (5, 10, 15% of m_H)
- Consider both ggF and VBF production modes, and $H \rightarrow WW^* \rightarrow e\nu\mu\nu$ final state
- Using Run 2 data with integrated luminosity of **13.2 fb^{-1} at 13 TeV**

Backgrounds:

- Largest are Top and *WW*: normalization factors derived from control regions (except VBF *WW* 2J)
- *W*+jets: from data using "fake factor" method (from SM $H \rightarrow WW^*$ analysis)
- Z+jets, other diboson, H125: small, predicted from simulation

ggF *WW* CR

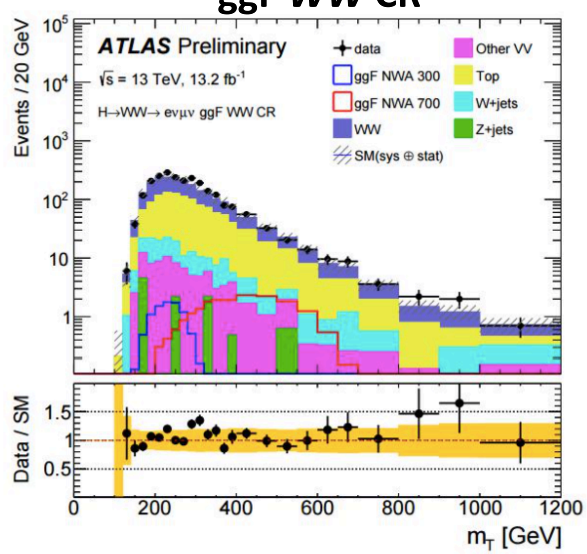

VBF Top CR

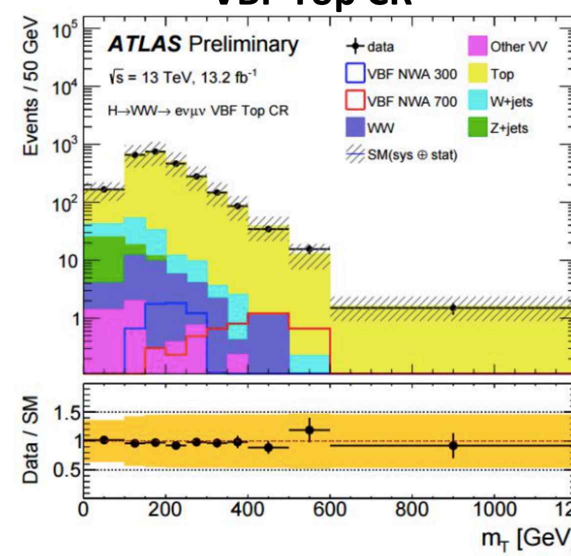

Signal regions:

- For first time use two VBF SRs: $\geq$2 jets SR with large m_{jj} and $|\Delta y_{jj}|$(<u>standard</u>), and 1-jet SR (<u>new</u>)
- ggF SR is then the quasi-inclusive rest

13 TeV High Mass Results

[ATLAS-CONF-2016-074]

- **No significant excess is found between 300 GeV and 3 TeV**
- Set 95% CL upper limits on:

$$\sigma_H \times BR(H \to WW)$$

ggF SR

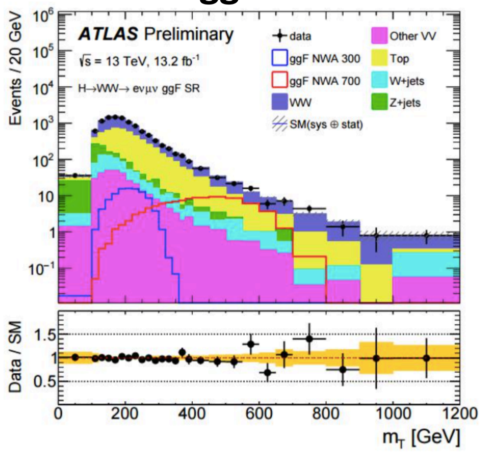

VBF 1J SR

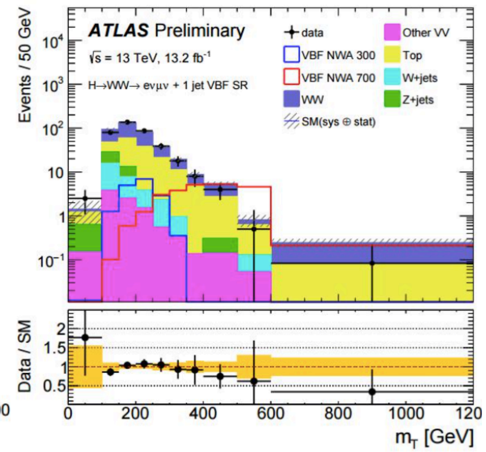

VBF 2J SR

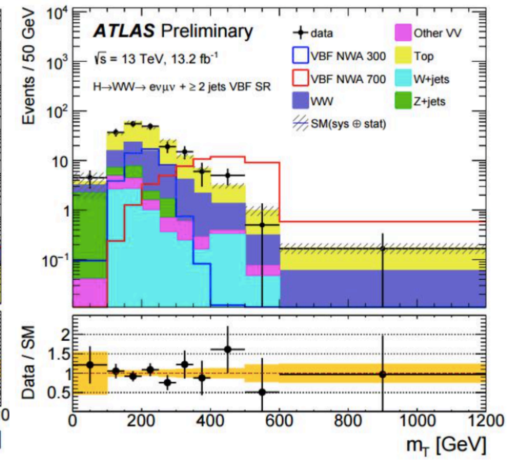

NWA, ggF

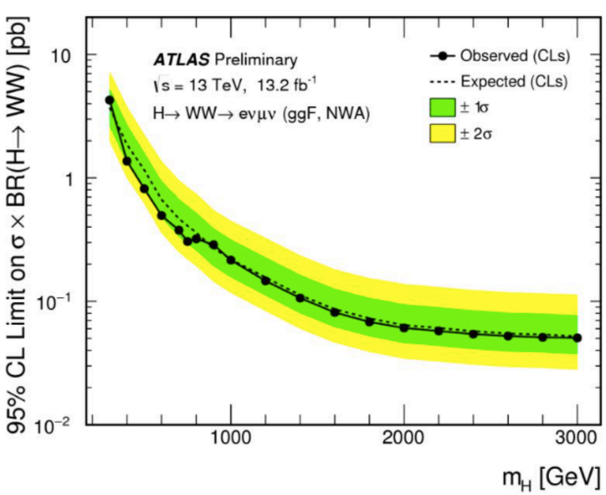

NWA, VBF

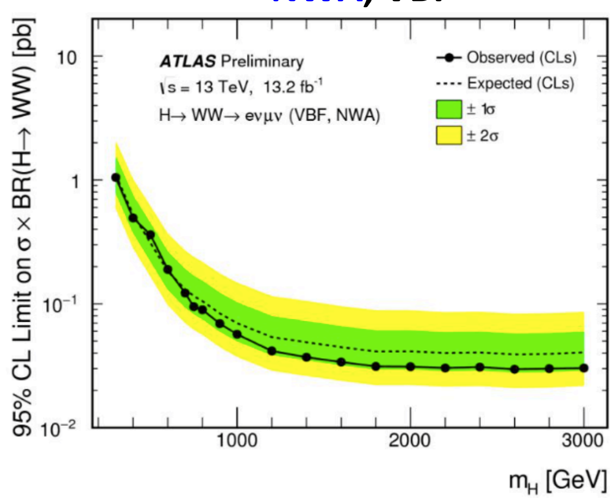

LWA, ggF

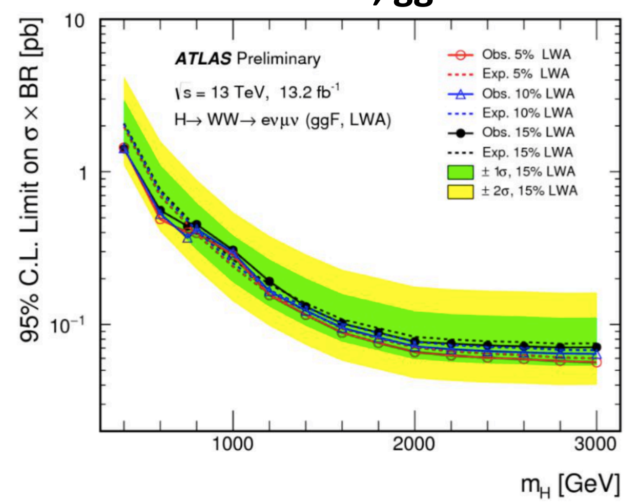

NWA: upper exclusion limits range from 4.3 pb (1.1 pb) at 300 GeV to 0.051 pb (0.03 pb) at 3 TeV for the ggF (VBF) analyses

LWA (15%): from 1.4pb at 400 GeV to 0.071 pb at 3 TeV

Summary

- $H \rightarrow WW^*$ plays an important role in Higgs boson property measurements, and searches for possible extended Higgs sectors
  - 4.2σ, 3.2σ and 2.5σ significance of ggF, VBF and *VH* production (6.5σ overall)
  - Rates and couplings consistent with SM expectation:

$$\mu = 1.16^{+0.16}_{-0.15}(\text{stat.})^{+0.18}_{-0.15}(\text{sys.}) \qquad |\kappa_V| = 1.06^{+0.10}_{-0.10} \qquad |\kappa_F| = 0.85^{+0.26}_{-0.20}$$

  - Spin/CP and differential cross sections measurements are also consistent with SM (more info in the backup)
  - 13 TeV high-mass search with no significant excess observed from 300 GeV – 3 TeV

- Future results with the Run 2 data will allow for more precise measurements and therefore more stringent tests of the SM predictions

- **So stay tuned!**

BACKUP

Spin and CP with $H \rightarrow WW^*$

Eur. Phys. J. C (2015)

- Follows closely the main ggF $H \rightarrow WW^* \rightarrow e\nu\mu\nu$ analysis
- Main spin/CP sensitive variables: m_{ll}, p^T_{ll}, $\Delta\phi_{ll}$, m_T
- Different BDTs trained for different spin/CP models
- Construct test statistic (q) to test particular J^P hypothesis against SM spin/CP assignment (0^+)

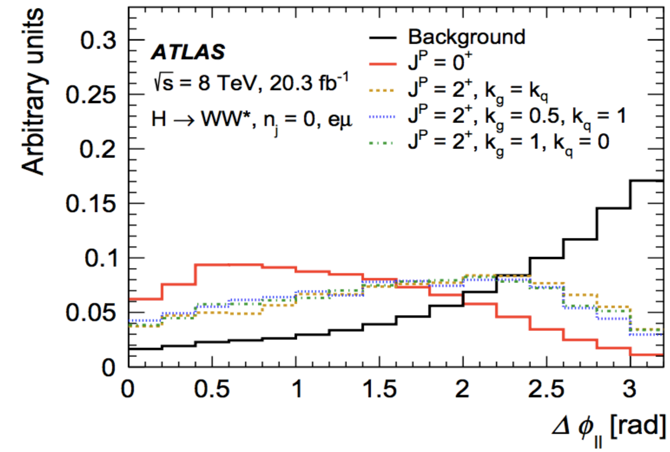

0^+ vs 2^+

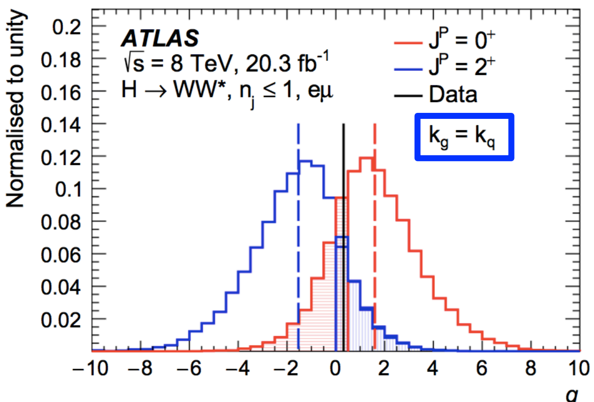

2^+ disfavored at 84.5% CL

(92.5-99.4% for $k_g \neq k_q$)

0^+ vs 0^-

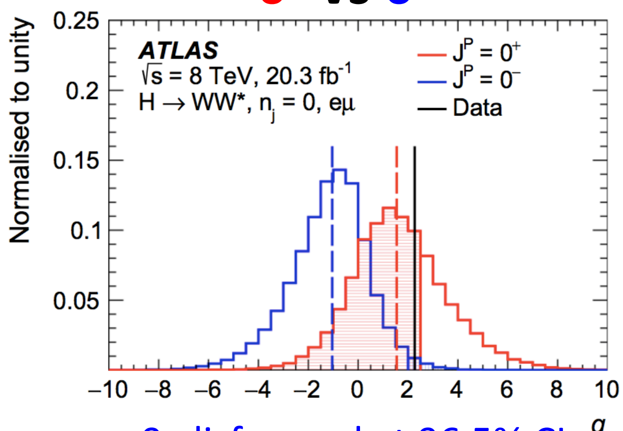

0^- disfavored at 96.5% CL

0^+ vs 0^+ BSM

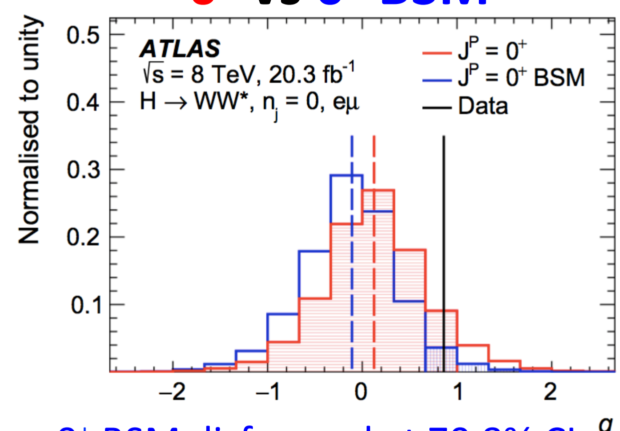

0^+ BSM disfavored at 70.8% CL

After combining *WW with the other channels (*ZZ, γγ*), the alternative spin/CP models are excluded at above 99% CL in favor of the 0^+ hypothesis.**

However a mixed state of CP-even and CP-odd is still allowed, with up to 30% mixing.

Differential Cross Section

arXiv:1604.02997

- Possible to directly measure several kinematic distributions in a close to model independent way
- Analysis follows closely the main ggF $H \rightarrow WW^{*} \rightarrow e\nu\mu\nu$ analysis
- Unfolding corrects measured distribution for detector effects and brings it from the signal (reconstructed) to the fiducial (truth level) volume

$$\frac{d\sigma}{dX_i} = \frac{1}{\mathcal{L} * BR} \frac{M_{ji}^{-1} \epsilon_{fid,j}}{\epsilon_{truth,sel,i}} (N_j - B_j)$$

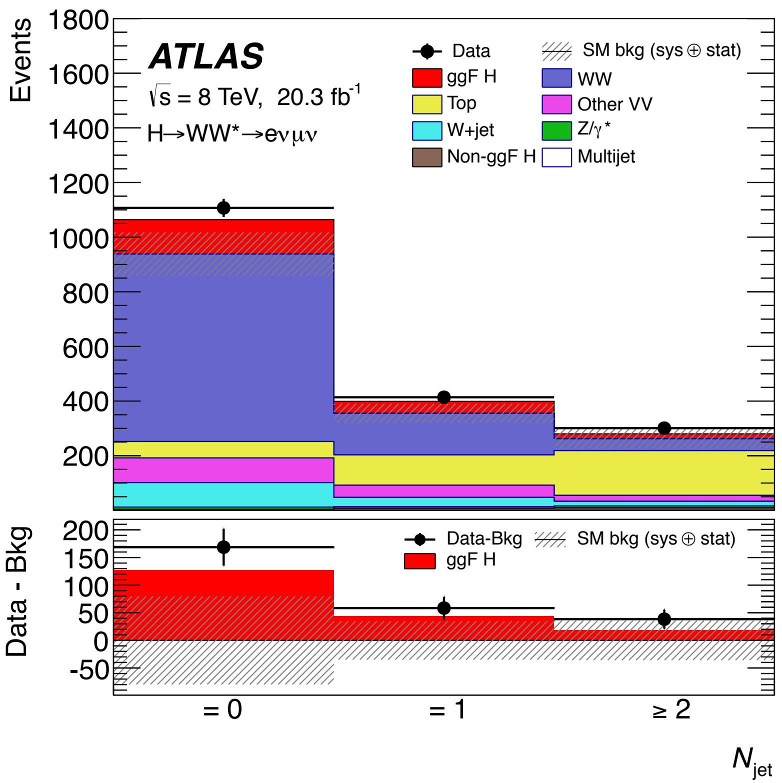

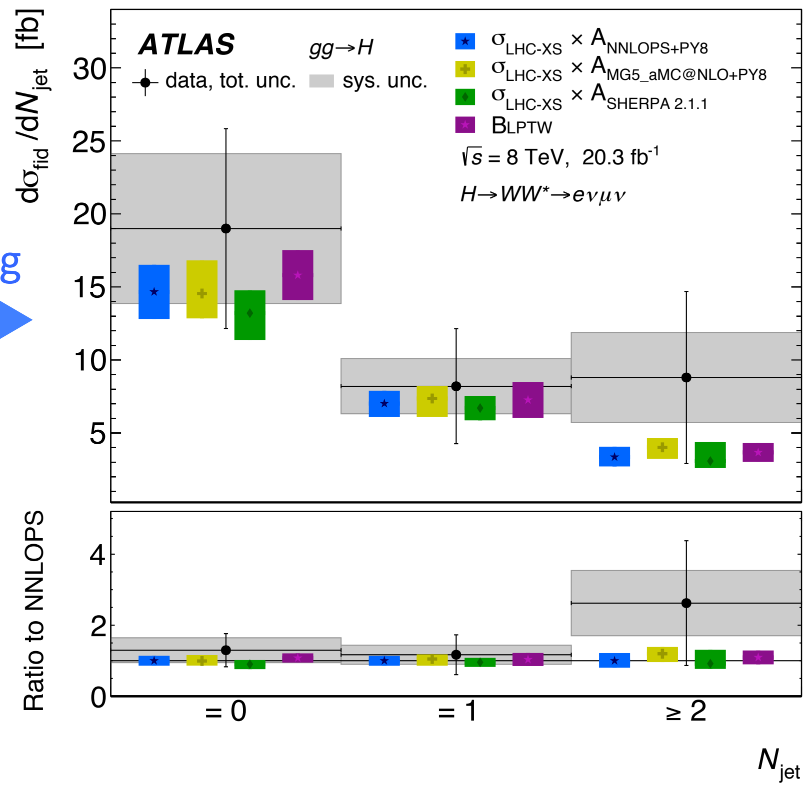

Production/decay rates and couplings

- Combination includes results from **H→γγ, ZZ***, **WW***, **ττ**, **bb̄**, **μμ**, **Zγ** analyses, and constraints on **ttH** and **off-shell** Higgs production. arXiv:1507.04548 (2015)

- **κ-framework**: search for deviations of SM Higgs coupling to other particles by introducing multipliers using ***tree-level motivated benchmark model*** following the LHC Higgs WG recommendations (arXiv:1307.1347)

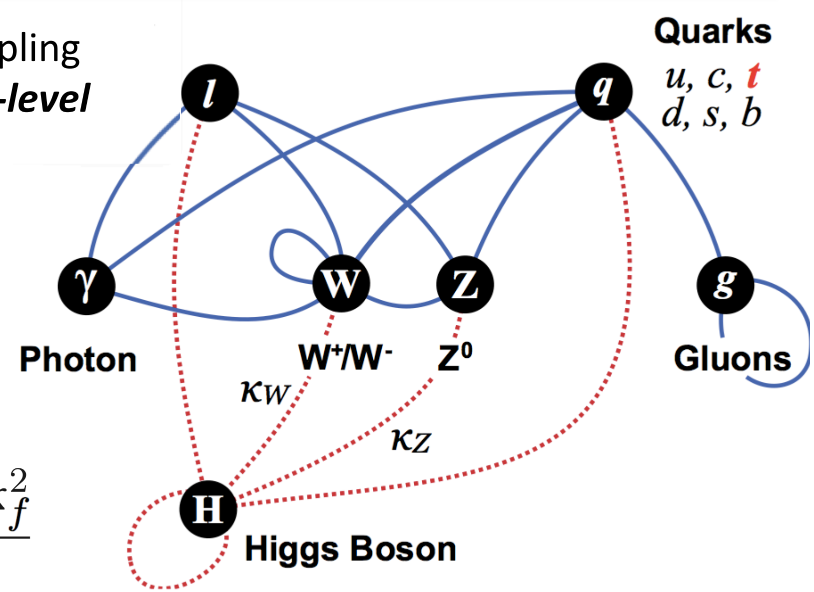

- Assumptions:
  - Single, narrow, CP-even scalar resonance (tensor structure of couplings assumed to be those of SM)
  - Narrow width approximation is valid:

$$\sigma\mathcal{B}(i \to H \to f) = \frac{\sigma_i \Gamma_f}{\Gamma_H} = \frac{\sigma_i^{SM}\Gamma_f^{SM}}{\Gamma_H^{SM}} \cdot \frac{\kappa_i^2 \cdot \kappa_f^2}{\kappa_H^2}$$

Parameters of interest:

- **Signal strength μ = σ×BR / (σ×BR)$_{SM}$**
  - the multiplier for total yield (can be defined for each production mode and decay channel)
- **Multipliers κ for a given coupling**
  - Different models tested by imposing different relations between multipliers
  - **κ** allows more direct access to coupling than μ (complex interplay between prod./decay)
- **In both cases, SM has μ = 1.0 and κ = 1.0**

Benchmark Coupling Models

- **Many test are possible, under different assumptions:**
  - ➢ **Allow/don't allow invisible decays (contribution to total width)**
  - ➢ **Allow/don't allow BSM particles in loops**

arXiv:1507.04548 (2015)

Table 10: Summary of benchmark coupling models considered in this paper, where $\lambda_{ij} \equiv \kappa_i/\kappa_j$, $\kappa_{ii} \equiv \kappa_i\kappa_i/\kappa_H$, and the functional dependence assumptions are: $\kappa_V = \kappa_W = \kappa_Z$, $\kappa_F = \kappa_t = \kappa_b = \kappa_\tau = \kappa_\mu$ (and similarly for the other fermions), $\kappa_g = \kappa_g(\kappa_b, \kappa_t)$, $\kappa_\gamma = \kappa_\gamma(\kappa_b, \kappa_t, \kappa_\tau, \kappa_W)$, and $\kappa_H = \kappa_H(\kappa_i)$. The tick marks indicate which assumptions are made in each case. The last column shows, as an example, the relative coupling strengths involved in the $gg \to H \to \gamma\gamma$ process.

Section in this paper	Corresponding table in Ref.[11]	Probed couplings	Parameters of interest	Functional assumptions κ_V	κ_F	κ_g	κ_γ	κ_H	Example: $gg \to H \to \gamma\gamma$
5.2.1	43.1	Couplings to fermions and bosons	κ_V, κ_F	✓	✓	✓	✓	✓	$\kappa_F^2 \cdot \kappa_\gamma^2(\kappa_F, \kappa_V)/\kappa_H^2(\kappa_F, \kappa_V)$
5.2.2	43.2		$\kappa_F, \kappa_V, \mathrm{BR}_{\mathrm{i.,u.}}$	≤ 1 –	– –	✓ ✓	✓ ✓	✓ $\kappa_{\mathrm{on}} = \kappa_{\mathrm{off}}$	$\frac{\kappa_F^2 \cdot \kappa_\gamma(\kappa_F,\kappa_V)^2}{\kappa_H^2(\kappa_F,\kappa_V)} \cdot (1 - \mathrm{BR}_{\mathrm{i.,u.}})$
5.2.3	43.3		$\lambda_{FV}, \kappa_{VV}$	✓	✓	✓	✓	–	$\kappa_{VV}^2 \cdot \lambda_{FV}^2 \cdot \kappa_\gamma^2(\lambda_{FV}, \lambda_{FV}, \lambda_{FV}, 1)$
5.3.1	46	Up-/down-type fermions	$\lambda_{du}, \lambda_{Vu}, \kappa_{uu}$	✓	κ_u, κ_d	✓	✓	–	$\kappa_{uu}^2 \cdot \kappa_g^2(\lambda_{du}, 1) \cdot \kappa_\gamma^2(\lambda_{du}, 1, \lambda_{du}, \lambda_{Vu})$
5.3.2	47	Leptons/quarks	$\lambda_{\ell q}, \lambda_{Vq}, \kappa_{qq}$	✓	κ_ℓ, κ_q	✓	✓	–	$\kappa_{qq}^2 \cdot \kappa_\gamma^2(1, 1, \lambda_{\ell q}, \lambda_{Vq})$
5.4.1	48.1	Vertex loops + $H \to$invisible/undetected decays	$\kappa_g, \kappa_\gamma, \kappa_{Z\gamma}$	=1	=1	–	–	✓	$\kappa_g^2 \cdot \kappa_\gamma^2/\kappa_H^2(\kappa_g, \kappa_\gamma)$
5.4.2	48.2		$\kappa_g, \kappa_\gamma, \kappa_{Z\gamma}, \mathrm{BR}_{\mathrm{i.,u.}}$	=1	=1	–	–	✓	$\kappa_g^2 \cdot \kappa_\gamma^2/\kappa_H^2(\kappa_g, \kappa_\gamma) \cdot (1 - \mathrm{BR}_{\mathrm{i.,u.}})$
5.4.3	49		$\kappa_F, \kappa_V, \kappa_g, \kappa_\gamma, \kappa_{Z\gamma}, \mathrm{BR}_{\mathrm{i.,u.}}$	≤ 1 –	– –	– –	– –	✓ $\kappa_{\mathrm{on}} = \kappa_{\mathrm{off}}$	$\frac{\kappa_F^2 \cdot \kappa_\gamma(\kappa_F,\kappa_V)^2}{\kappa_H^2(\kappa_F,\kappa_V,\kappa_g,\kappa_\gamma)} \cdot (1 - \mathrm{BR}_{\mathrm{i.,u.}})$
5.5.1	51	Generic models with and without assumptions on vertex loops and Γ_H	$\kappa_W, \kappa_Z, \kappa_t, \kappa_b, \kappa_\tau, \kappa_\mu$	–	–	✓	✓	✓	$\frac{\kappa_g^2(\kappa_b,\kappa_t) \cdot \kappa_\gamma^2(\kappa_b,\kappa_t,\kappa_\tau,\kappa_\mu,\kappa_W)}{\kappa_H^2(\kappa_b,\kappa_t,\kappa_\tau,\kappa_\mu,\kappa_W,\kappa_Z)}$
5.5.2	50.2		$\kappa_W, \kappa_Z, \kappa_t, \kappa_b, \kappa_\tau, \kappa_\mu, \kappa_g, \kappa_\gamma, \kappa_{Z\gamma}, \mathrm{BR}_{\mathrm{i.,u.}}$	≤ 1 – –	– – –	– – –	– – –	✓ ✓ $\kappa_{\mathrm{on}} = \kappa_{\mathrm{off}}$	$\frac{\kappa_g^2 \cdot \kappa_\gamma^2}{\kappa_H^2(\kappa_b,\kappa_t,\kappa_\tau,\kappa_\mu,\kappa_W,\kappa_Z)} \cdot (1 - \mathrm{BR}_{\mathrm{i.,u.}})$
5.5.3	50.3		$\lambda_{WZ}, \lambda_{tg}, \lambda_{bZ}, \lambda_{\tau Z}, \lambda_{gZ}, \lambda_{\gamma Z}, \lambda_{(Z\gamma)Z}, \kappa_{gZ}$	–	–	–	–	–	$\kappa_{gZ}^2 \cdot \lambda_{\gamma Z}^2$

Triggers

TABLE II. Summary of the minimum lepton p_T trigger requirements (in GeV) during the 8 TeV data-taking. For single-electron triggers, the hardware and software thresholds are either 18 and 24i or 30 and 60, respectively. The "i" denotes an isolation requirement that is less restrictive than the isolation requirement imposed in the offline selection. For dilepton triggers, the pair of thresholds corresponds to the leading and subleading lepton, respectively; the "μ, μ" dilepton trigger requires only a single muon at level-1. The "and" and "or" are logical.

Name	Level-1 trigger	High-level trigger
Single lepton		
e	18 or 30	24i or 60
μ	15	24i or 36
Dilepton		
e, e	10 and 10	12 and 12
μ, μ	15	18 and 8
e, μ	10 and 6	12 and 8

MC samples

Process	Generator	$\sigma(\times\mathrm{Br})$ [pb]	Cross-section normalisation
Higgs boson			
VH $(H\to WW^*)$	PYTHIA [25, 26] v8.165, v6.428	0.24, 0.20	NNLO QCD + NLO EW
VH $(H\to\tau\tau)$	PYTHIA v8.165, v6.428	0.07, 0.06	NNLO QCD + NLO EW
$gg\to H$ $(H\to WW^*)$	POWHEG-BOX [27–30] v1.0 (r1655)+ PYTHIA v8.165, v6.428	4.1, 3.3	NNLO+NNLL QCD + NLO EW
VBF $(H\to WW^*)$	POWHEG-BOX [31] v1.0 (r1655)+ PYTHIA v8.165, v6.428	0.34, 0.26	NNLO QCD + NLO EW
$t\bar{t}$H $(H\to WW^*)$	PYTHIA v8.165	0.028, 0.019	NLO
Single boson			
$Z/\gamma^*(\to\ell\ell)$+jets ($m_{\ell\ell}>10$ GeV)	ALPGEN [32] v2.14 + HERWIG [33] v6.52	16540, 12930	NNLO
HF $Z/\gamma^*(\to\ell\ell)$+jets ($m_{\ell\ell}>30$ GeV)	ALPGEN v2.14 + HERWIG v6.52	126, 57	NNLO
VBF $Z/\gamma^*(\to\ell\ell)$ ($m_{\ell\ell}>7$ GeV)	SHERPA [34] v1.4.1	5.3, 2.8	LO
Top-quark			
$t\bar{t}$	POWHEG-BOX [35] v1.0 (r2129)+PYTHIA v6.428	250, 180	NNLO+NNLL
	MC@NLO [36] v4.03		
$t\bar{t}W/Z$	MADGRAPH [37] v5.1.5.2, v5.1.3.28 +PYTHIA v6.428	0.35, 0.25	LO
tqb	ACERMC [38] v3.8 +PYTHIA v6.428	88, 65	NNLL
tb, tW	POWHEG-BOX [39, 40] v1.0 (r2092)+ PYTHIA v6.428	28, 20	NNLL
tZ	MADGRAPH v5.1.5.2, v5.1.5.11 +PYTHIA v6.428	0.035, 0.025	LO
Dibosons			
$WZ/W\gamma^*(\to\ell\ell\ell\nu)(m_{\ell\ell}>7$ GeV)	POWHEG-BOX [41] v1.0 (r1508)+PYTHIA v8.165, v6.428	12.7, 10.7	NLO
$WZ/W\gamma^*(\to\ell\ell\ell\nu)$(min. $m_{\ell\ell}<7$ GeV)	SHERPA v1.4.1	12.2, 10.5	NLO
other WZ	POWHEG-BOX [41] v1.0 (r1508) + PYTHIA v8.165	21.2, 17.2	NLO
$q\bar{q}/qg\to Z^{(*)}Z^{(*)}(\to\ell\ell\ell\ell,\ell\ell\nu\nu)$ ($m_{\ell\ell}>4$ GeV)	POWHEG-BOX [41] v1.0 (r1556) +PYTHIA v8.165, v6.428	1.24, 0.79	NLO
$q\bar{q}/qg\to Z^{(*)}Z^{(*)}(\to\ell\ell\ell\ell,\ell\ell\nu\nu)$ (min. $m_{\ell\ell}<4$ GeV)	SHERPA v1.4.1	7.3, 5.9	NLO
other $q\bar{q}/qg\to ZZ$	POWHEG-BOX [41] v1.0 (r1556) + PYTHIA v8.165	6.9, 5.7	NLO
$gg\to Z^{(*)}Z^{(*)}$	gg2ZZ [42] v3.1.2 + HERWIG v6.52 (8 TeV only)	0.59	LO
$q\bar{q}/qg\to WW$	POWHEG-BOX [41] v1.0 (r1556) + PYTHIA v6.428	54, 45	NLO
	SHERPA v1.4.1 (for 2ℓ-DFOS 8 TeV only)	54	NLO
$gg\to WW$	gg2WW [43] v3.1.2 + HERWIG v6.52	1.9, 1.1	LO
VBS WZ, $ZZ(\to\ell\ell\ell\ell,\ell\ell\nu\nu)$ ($m_{\ell\ell}>7$ GeV), WW	SHERPA v1.4.1	1.2, 0.88	LO
$W\gamma$ ($p_{\mathrm{T}}^{\gamma}>8$ GeV)	ALPGEN v2.14 +HERWIG v6.52	1140, 970	NLO
$Z\gamma$ ($p_{\mathrm{T}}^{\gamma}>8$ GeV)	SHERPA v1.4.3	960, 810	NLO
Tribosons			
$WWW^*, ZWW^*, ZZZ^*, WW\gamma^*$	MADGRAPH v5.1.3.33, v5.1.5.10 + PYTHIA v6.428	0.44, 0.18	NLO

SR event selections

TABLE IV. Event selection summary. Selection requirements specific to the $e\mu$ and $ee/\mu\mu$ lepton-flavor samples are noted as such (otherwise, they apply to both); a dash (-) indicates no selection. For the $n_j \geq 2$ VBF-enriched category, MET denotes all types of missing transverse momentum observables. Values are given for the analysis of 8 TeV data for $m_H = 125$ GeV; the modifications for 7 TeV are given in Sec. IV E. All energy-related values are in GeV.

		ggF-enriched			VBF-enriched
Objective		$n_j = 0$	$n_j = 1$	$n_j \geq 2$ ggF	$n_j \geq 2$ VBF
Preselection	All n_j	$p_T^{\ell 1} > 22$ for the leading lepton ℓ_1 $p_T^{\ell 2} > 10$ for the subleading lepton ℓ_2 Opposite-charge leptons $m_{\ell\ell} > 10$ for the $e\mu$ sample $m_{\ell\ell} > 12$ for the $ee/\mu\mu$ sample $\lvert m_{\ell\ell} - m_Z \rvert > 15$ for the $ee/\mu\mu$ sample			
		$p_T^{\text{miss}} > 20$ for $e\mu$ $E_{T,\text{rel}}^{\text{miss}} > 40$ for $ee/\mu\mu$	$p_T^{\text{miss}} > 20$ for $e\mu$ $E_{T,\text{rel}}^{\text{miss}} > 40$ for $ee/\mu\mu$	$p_T^{\text{miss}} > 20$ for $e\mu$ -	No MET requirement for $e\mu$ -
Reject backgrounds	DY	$p_{T,\text{rel}}^{\text{miss (trk)}} > 40$ for $ee/\mu\mu$ $f_{\text{recoil}} < 0.1$ for $ee/\mu\mu$ $p_T^{\ell\ell} > 30$ $\Delta\phi_{\ell\ell,\text{MET}} > \pi/2$	$p_{T,\text{rel}}^{\text{miss (trk)}} > 35$ for $ee/\mu\mu$ $f_{\text{recoil}} < 0.1$ for $ee/\mu\mu$ $m_{\tau\tau} < m_Z - 25$ -	- - $m_{\tau\tau} < m_Z - 25$ -	$p_T^{\text{miss}} > 40$ for $ee/\mu\mu$ $E_T^{\text{miss}} > 45$ for $ee/\mu\mu$ $m_{\tau\tau} < m_Z - 25$ -
	Misid	-	$m_T^{\ell} > 50$ for $e\mu$	-	-
	Top	$n_j = 0$ - -	$n_b = 0$ - -	$n_b = 0$ - -	$n_b = 0$ p_T^{sum} inputs to BDT $\Sigma m_{\ell j}$ inputs to BDT
VBF topology		-	-	See Sec. IV D for rejection of VBF & VH ($W, Z \to jj$), where $H \to WW^*$	m_{jj} inputs to BDT Δy_{jj} inputs to BDT ΣC_ℓ inputs to BDT $C_{\ell 1} < 1$ and $C_{\ell 2} < 1$ $C_{j3} > 1$ for j_3 with $p_T^{j3} > 20$ $O_{\text{BDT}} \geq -0.48$
$H \to WW^* \to \ell\nu\ell\nu$ decay topology		$m_{\ell\ell} < 55$ $\Delta\phi_{\ell\ell} < 1.8$ No m_T requirement	$m_{\ell\ell} < 55$ $\Delta\phi_{\ell\ell} < 1.8$ No m_T requirement	$m_{\ell\ell} < 55$ $\Delta\phi_{\ell\ell} < 1.8$ No m_T requirement	$m_{\ell\ell}$ inputs to BDT $\Delta\phi_{\ell\ell}$ inputs to BDT m_T inputs to BDT

m_T in $\geq$2 jet ggF SR

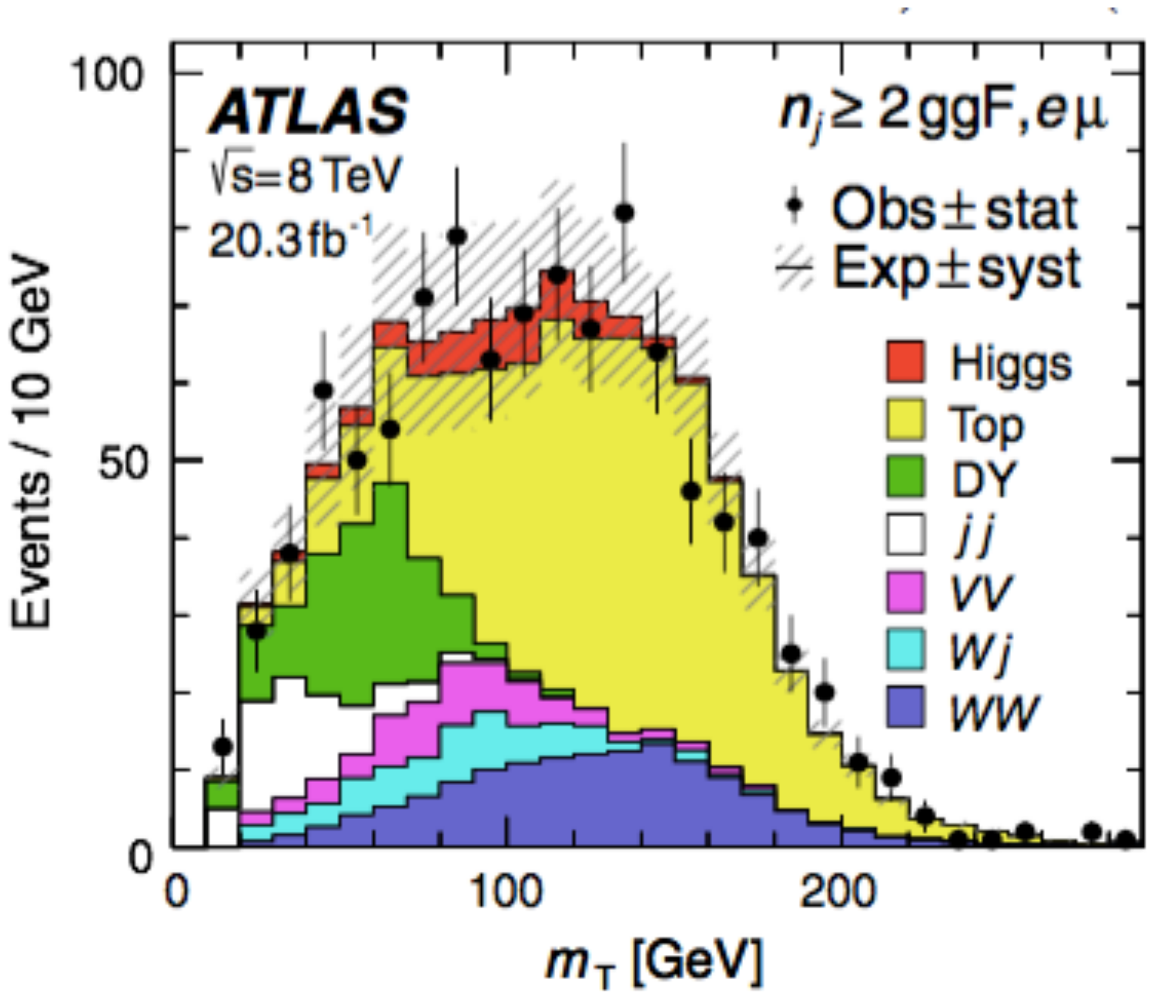

SR plots for VBF BDT analysis

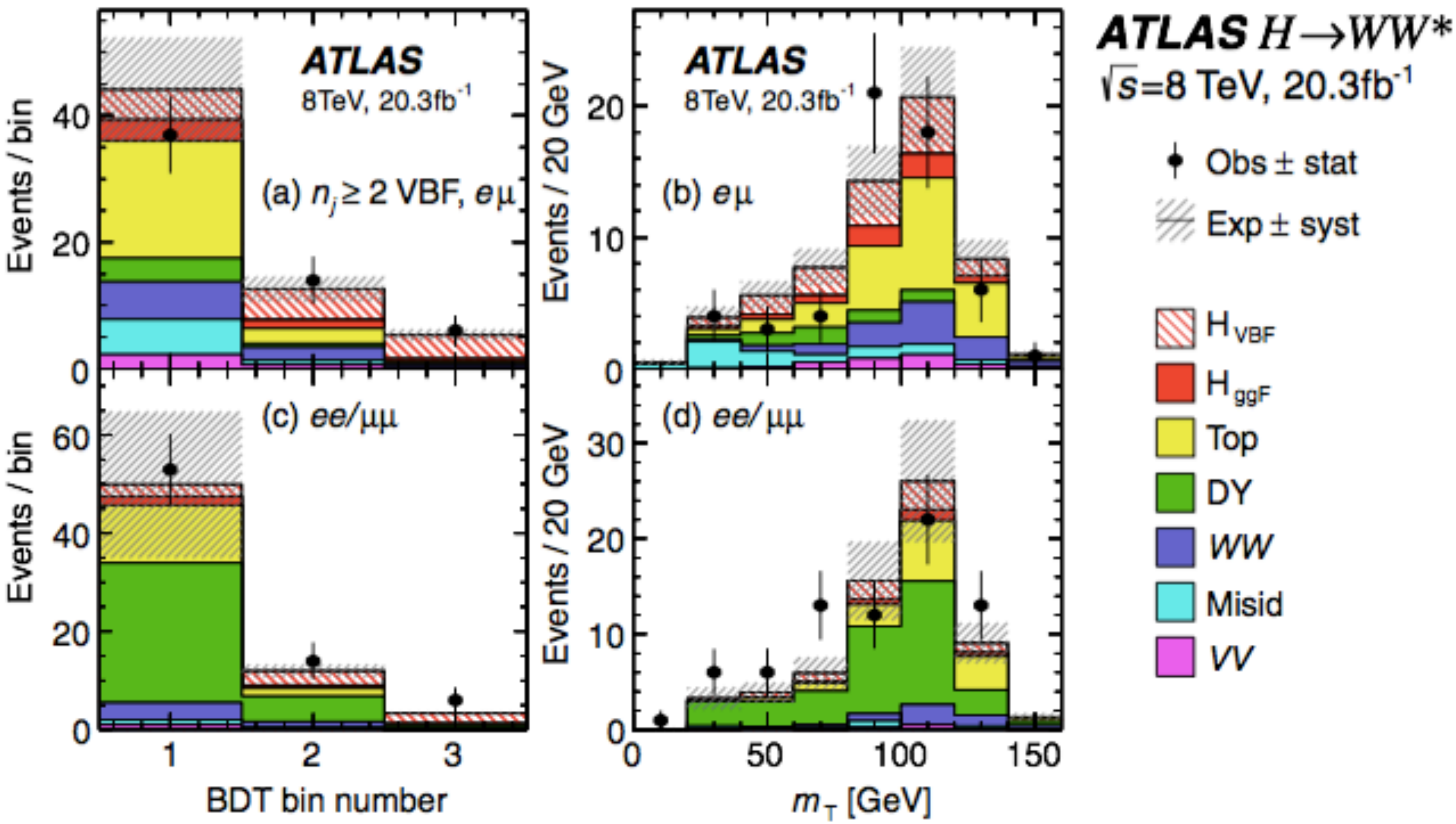

VBF cross-check analysis

- Note: for VBF a cross-check analyses is performed in parallel to the BDT, using sequential selections (cut-based) on some of the variables used as inputs to the BDT.

TABLE VII. Event selection for the $n_j \geq 2$ VBF-enriched category in the 8 TeV cross-check data analysis (see Table V for presentation details). The N_{ggF}, N_{VBF}, and N_{VH} expected yields are shown separately. The expected yields for WW and $Z/\gamma^* \to \tau\tau$ are divided into QCD and electroweak (EW) processes, where the latter includes VBS or VBF production.

	Summary						Composition of N_{bkg}									
				N_{signal}			N_{WW}		N_{top}		N_{misid}			$N_{\mathrm{Drell\text{-}Yan}}$		
Selection	$N_{\mathrm{obs}}/N_{\mathrm{bkg}}$	N_{obs}	N_{bkg}	N_{ggF}	N_{VBF}	N_{VH}	N_{WW}^{QCD}	N_{WW}^{EW}	$N_{t\bar{t}}$	N_{t}	N_{Wj}	N_{jj}	N_{VV}	$N_{ee/\mu\mu}$	$N_{\tau\tau}^{\mathrm{QCD}}$	$N_{\tau\tau}^{\mathrm{EW}}$
$e\mu$ sample	1.00 ± 0.00	61434	61180	85	32	26	1350	68	51810	2970	847	308	380	51	3260	46
$n_b = 0$	1.02 ± 0.01	7818	7700	63	26	16	993	43	3000	367	313	193	273	35	2400	29
$p_{\mathrm{T}}^{\mathrm{sum}} < 15$	1.03 ± 0.01	5787	5630	46	23	13	781	38	1910	270	216	107	201	27	2010	23
$m_{\tau\tau} < m_Z - 25$	1.05 ± 0.02	3129	2970	40	20	9.9	484	22	1270	177	141	66	132	7.6	627	5.8
$m_{jj} > 600$	1.31 ± 0.12	131	100	2.3	8.2	-	18	8.9	40	5.3	1.8	2.4	5.1	0.1	15	1.0
$\Delta y_{jj} > 3.6$	1.33 ± 0.13	107	80	2.1	7.9	-	11.7	6.9	35	5.0	1.6	2.3	3.3	-	11.6	0.8
$C_{j3} > 1$	1.36 ± 0.18	58	43	1.3	6.6	-	6.9	5.6	14	3.0	1.3	1.3	2.0	-	6.8	0.6
$C_{\ell 1} < 1$, $C_{\ell 2} < 1$	1.42 ± 0.20	51	36	1.2	6.4	-	5.9	5.2	10.8	2.5	1.3	1.3	1.6	-	5.7	0.6
$m_{\ell\ell}$, $\Delta\phi_{\ell\ell}$, m_{T}	2.53 ± 0.71	14	5.5	0.8	4.7	-	1.0	0.5	1.1	0.3	0.3	0.3	0.6	-	0.5	0.2
$ee/\mu\mu$ sample	0.99 ± 0.01	26949	27190	31	14	10.1	594	37	23440	1320	230	8.6	137	690	679	16
n_b, $p_{\mathrm{T}}^{\mathrm{sum}}$, $m_{\tau\tau}$	1.03 ± 0.03	1344	1310	13	8.0	4.0	229	12.0	633	86	26	0.9	45	187	76	1.5
m_{jj}, Δy_{jj}, C_{j3}, C_ℓ	1.39 ± 0.28	26	19	0.4	2.9	0.0	3.1	3.1	5.5	1.0	0.2	0.0	0.7	3.8	0.7	0.1
$m_{\ell\ell}$, $\Delta\phi_{\ell\ell}$, m_{T}	1.63 ± 0.69	6	3.7	0.3	2.2	0.0	0.4	0.2	0.6	0.2	0.2	0.0	0.1	1.5	0.3	0.1

VH channels

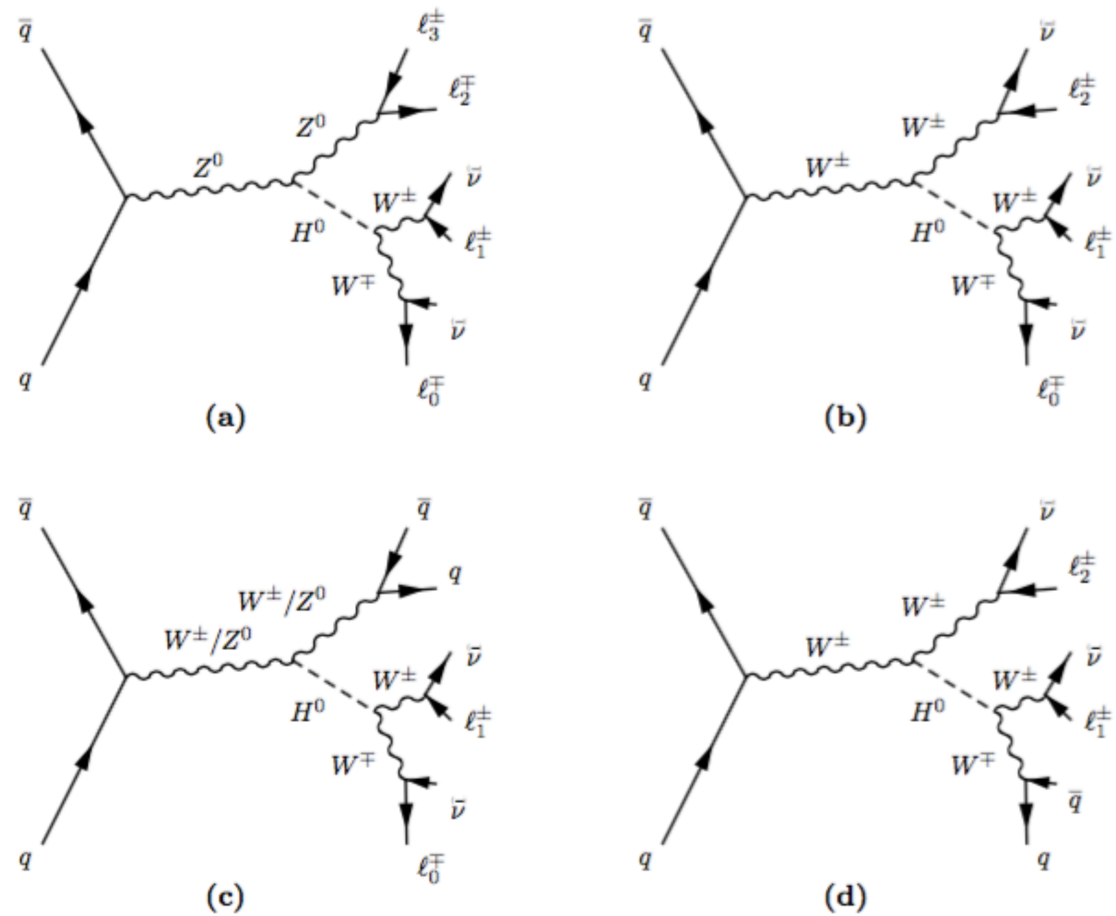

Figure 1. Tree-level Feynman diagrams of the $VH(H \to WW^*)$ topologies studied in this analysis: (a) 4ℓ channel (b) 3ℓ channel (c) opposite-sign 2ℓ channel and (d) same-sign 2ℓ channel. For charged lepton external lines, the directions of arrows refer to the superscripted sign. Relevant arrows are assigned to the associated neutrino external lines.

VH event selections

Channel	4ℓ		3ℓ			2ℓ		
Category	2SFOS	1SFOS	3SF	1SFOS	0SFOS	DFOS	SS2jet	SS1jet
Trigger	single-lepton triggers		single-lepton triggers			single-lepton & dilepton triggers		
Num. of leptons	4	4	3	3	3	2	2	2
$p_{\mathrm{T,leptons}}$ [GeV]	$> 25, 20, 15$	$> 25, 20, 15$	> 15	> 15	> 15	$> 22, 15$	$> 22, 15$	$> 22, 15$
Total lepton charge	0	0	± 1	± 1	± 1	0	± 2	± 2
Num. of SFOS pairs	2	1	2	1	0	0	0	0
Num. of jets	≤ 1	≤ 1	≤ 1	≤ 1	≤ 1	≥ 2	2	1
$p_{\mathrm{T,jets}}$ [GeV]	> 25 (30)	> 25 (30)	> 25 (30)	> 25 (30)	> 25 (30)	> 25 (30)	> 25 (30)	> 25 (30)
Num. of b-tagged jets	0	0	0	0	0	0	0	0
$E_{\mathrm{T}}^{\mathrm{miss}}$ [GeV]	> 20	> 20	> 30	> 30	—	> 20	> 50	> 45
$p_{\mathrm{T}}^{\mathrm{miss}}$ [GeV]	> 15	> 15	> 20	> 20	—	—	—	—
$\lvert m_{\ell\ell} - m_Z \rvert$ [GeV]	< 10 ($m_{\ell_2\ell_3}$)	< 10 ($m_{\ell_2\ell_3}$)	> 25	> 25	—	—	> 15	> 15
Min. $m_{\ell\ell}$ [GeV]	> 10 ($m_{\ell_0\ell_1}$)	> 10 ($m_{\ell_0\ell_1}$)	> 12	> 12	> 6	> 10	> 12 ($ee, \mu\mu$) > 10 ($e\mu$)	> 12 ($ee, \mu\mu$) > 10 ($e\mu$)
Max. $m_{\ell\ell}$ [GeV]	< 65 ($m_{\ell_0\ell_1}$)	< 65 ($m_{\ell_0\ell_1}$)	< 200	< 200	< 200	< 50	—	—
$m_{4\ell}$ [GeV]	> 140	—	—	—	—	—	—	—
$p_{\mathrm{T},4\ell}$ [GeV]	> 30	—	—	—	—	—	—	—
$m_{\tau\tau}$ [GeV]	—	—	—	—	—	$< (m_Z - 25)$	—	—
$\Delta R_{\ell_0\ell_1}$	—	—	< 2.0	< 2.0	—	—	—	—
$\Delta\phi_{\ell_0\ell_1}$ [rad]	< 2.5 ($\Delta\phi_{\ell_0\ell_1}^{\mathrm{boost}}$)	< 2.5 ($\Delta\phi_{\ell_0\ell_1}^{\mathrm{boost}}$)	—	—	—	< 1.8	—	—
m_{T} [GeV]	—	—	—	—	—	< 125	—	> 105 ($m_{\mathrm{T}}^{\mathrm{lead}}$)
Min. $m_{\ell_i j(j)}$ [GeV]	—	—	—	—	—	—	< 115	< 70
Min. $\phi_{\ell_i j}$ [rad]	—	—	—	—	—	—	< 1.5	< 1.5
Δy_{jj}	—	—	—	—	—	< 1.2	—	—
$\lvert m_{jj} - 85 \rvert$ [GeV]	—	—	—	—	—	< 15	—	—

Table 2. Definition of each signal region in this analysis. $m_{\mathrm{T}}^{\mathrm{lead}}$ is the transverse mass of the leading lepton and the $\mathbf{E}_{\mathrm{T}}^{\mathrm{miss}}$ (see section 5.2.4 for the definition of $m_{\mathrm{T}}^{\mathrm{lead}}$). For $p_{\mathrm{T,leptons}}$ in the 4ℓ channel the three values listed above refer to the leading, sub-leading, and to the two remaining leptons, respectively. For $p_{\mathrm{T,leptons}}$ in the 2ℓ channel the two values listed above refer to the leading and sub-leading leptons, respectively. For $p_{\mathrm{T,jets}}$ the value in parentheses refers to forward jets ($|\eta| > 2.4$).

BDT output in 3SF and 1SFOS SRs

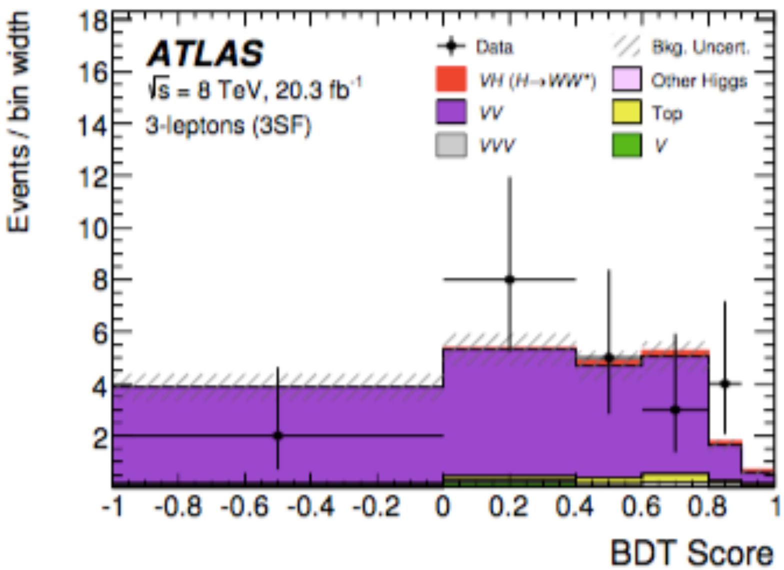

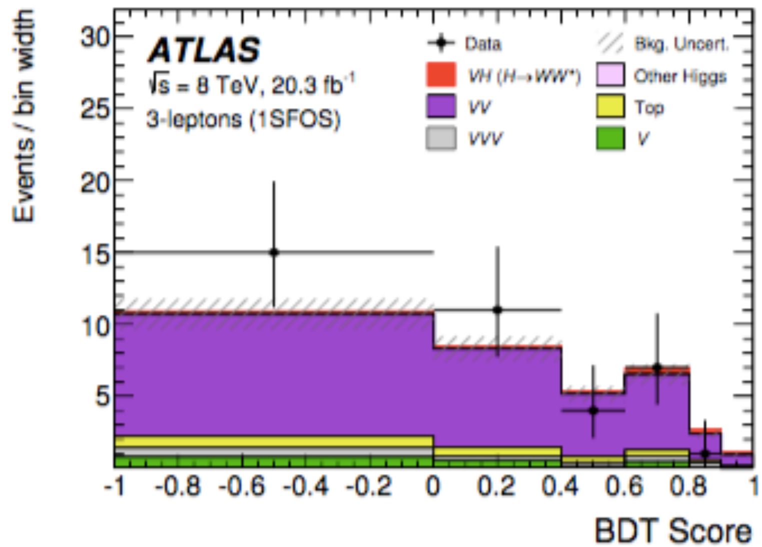

Variable definitions

$$m_{\mathrm{T}} = \sqrt{(E_{\mathrm{T}}^{\ell\ell} + p_{\mathrm{T}}^{\nu\nu})^2 - |\boldsymbol{p}_{\mathrm{T}}^{\ell\ell} + \boldsymbol{p}_{\mathrm{T}}^{\nu\nu}|^2}, \tag{1}$$

where $E_{\mathrm{T}}^{\ell\ell} = \sqrt{(p_{\mathrm{T}}^{\ell\ell})^2 + (m_{\ell\ell})^2}$, $\boldsymbol{p}_{\mathrm{T}}^{\nu\nu}$ ($\boldsymbol{p}_{\mathrm{T}}^{\ell\ell}$) is the vector sum of the neutrino (lepton) transverse momenta, and $p_{\mathrm{T}}^{\nu\nu}$ ($p_{\mathrm{T}}^{\ell\ell}$) is its modulus. The distribution has a kinematic upper edge at m_H, but in practice can exceed it because of detector resolution.

$$m_{\mathrm{T}}^{\ell_i} = \sqrt{2 p_{\mathrm{T}}^{\ell_i} \cdot p_{\mathrm{T}}^{\mathrm{miss}} \cdot (1 - \cos \Delta\phi)}, \tag{5}$$

where $\Delta\phi$ is the angle between the lepton transverse momentum and $\boldsymbol{p}_{\mathrm{T}}^{\mathrm{miss}}$. This quantity tends to have small

$$E_{\mathrm{T,rel}}^{\mathrm{miss}} = \begin{cases} E_{\mathrm{T}}^{\mathrm{miss}} \sin \Delta\phi_{\mathrm{near}} & \text{if } \Delta\phi_{\mathrm{near}} < \pi/2 \\ E_{\mathrm{T}}^{\mathrm{miss}} & \text{otherwise,} \end{cases} \tag{3}$$

where $\Delta\phi_{\mathrm{near}}$ is the azimuthal separation of the $\boldsymbol{E}_{\mathrm{T}}^{\mathrm{miss}}$ and the nearest high-p_{T} lepton or jet. A similar calculation defines $p_{\mathrm{T,rel}}^{\mathrm{miss}}$ and $p_{\mathrm{T,rel}}^{\mathrm{miss\,(trk)}}$.

suppress such mismeasured DY events, jets with $p_{\mathrm{T}}^{j} > 10$ GeV, within a $\pi/2$ wedge in ϕ (noted as $\wedge$) centered on $-\boldsymbol{p}_{\mathrm{T}}^{\ell\ell}$, are used to define a fractional jet recoil relative to the dilepton transverse momentum:

$$f_{\mathrm{recoil}} = \left| \sum_{\text{jets } j \text{ in } \wedge} \mathrm{JVF}_j \cdot \boldsymbol{p}_{\mathrm{T}}^{j} \right| \Big/ p_{\mathrm{T}}^{\ell\ell}. \tag{4}$$

The central-jet veto uses jets with $p_{\mathrm{T}} > 20$ GeV, and this requirement is applied in both the BDT and cross-check analyses. The selection can be expressed in terms of jet centrality, defined as

$$C_{j3} = \left| \eta_{j3} - \frac{\Sigma \eta_{jj}}{2} \right| \Big/ \frac{\Delta \eta_{jj}}{2}, \tag{6}$$

WW background

- Same selections as SR but without $\Delta\phi_{ll}$ cut
- For $N_j = 0$: CR with $55 < m_{ll} < 110$ GeV
- For $N_j = 1$: CR with $m_{ll} > 80$ GeV
- For $N_j \geq 2$: taken from MC (with validation region)

- NFs from the fit:

$$\beta_{WW}^{0j} = 1.22 \pm 0.03(\mathrm{stat}) \pm 0.10(\mathrm{syst})$$

$$\beta_{WW}^{1j} = 1.05 \pm 0.05(\mathrm{stat}) \pm 0.24(\mathrm{syst})$$

- WW theory uncert. on extrapolation factor

	$n_j = 0$						$n_j = 1$
SR category	Scale	PDF	Gen	EW	UE/PS	Total	Total
SR $e\mu$, $10 < m_{\ell\ell} < 30$							
$p_T^{\ell 2} > 20$	0.7	0.6	3.1	−0.3	−1.9	3.8	7.1
$15 < p_T^{\ell 2} \leq 20$	1.2	0.8	0.9	0.7	1.7	2.6	3.9
$10 < p_T^{\ell 2} \leq 15$	0.7	1.0	0.4	1.2	2.2	2.8	5.4
SR $e\mu$, $30 < m_{\ell\ell} < 55$							
$p_T^{\ell 2} > 20$	0.8	0.7	3.9	−0.4	−2.4	4.8	7.1
$15 < p_T^{\ell 2} \leq 20$	0.8	0.7	1.0	0.5	1.0	2.0	4.5
$10 < p_T^{\ell 2} \leq 15$	0.7	0.8	0.5	0.8	1.5	2.1	4.5
SR $ee/\mu\mu$, $12 < m_{\ell\ell} < 55$							
$p_T^{\ell 2} > 10$	0.8	1.1	2.4	0.1	−1.2	2.9	5.1

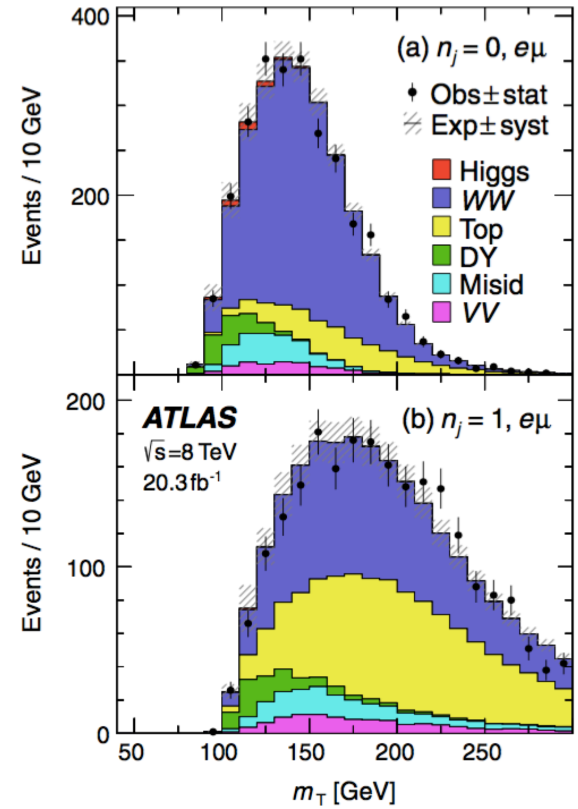

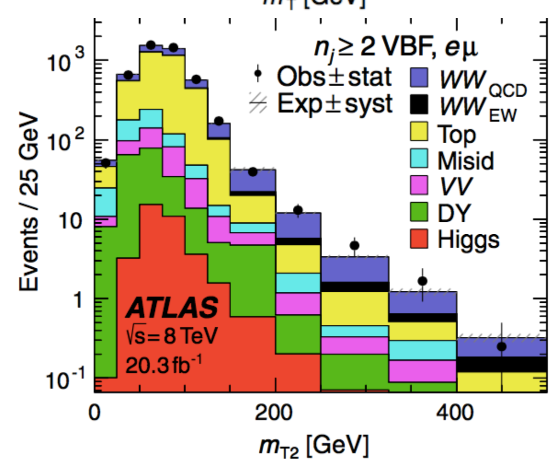

Top background (1)

- **<u>For $N_j = 0$: using CR (jet inclusive)</u>**
  - Extrapolated factor from MC (SR and jet inclusive CR) corrected using data in sample with $N_b \geq 1$

$$B^{\mathrm{est}}_{\mathrm{top},0j} = N_{\mathrm{CR}} \cdot \underbrace{B_{\mathrm{SR}}/B_{\mathrm{CR}}}_{\alpha^{0j}_{\mathrm{MC}}} \cdot \underbrace{(\alpha^{1b}_{\mathrm{data}}/\alpha^{1b}_{\mathrm{MC}})^2}_{\gamma_{1b}}$$

correction factor

- Uncertainties on extrapolation procedure:

Uncertainty source	$\alpha^{0j}_{\mathrm{MC}}/(\alpha^{1b}_{\mathrm{MC}})^2$	ϵ_{rest}	Total
(a) $n_j = 0$			
Experimental	4.4	1.2	4.6
Non-top-quark subtraction	-	-	2.7
Theoretical	3.9	4.5	4.9
Statistical	2.2	0.7	2.3
Total	6.8	4.7	7.6

- Resulting NFs and correction factor:

$$\beta^{0j}_{\mathrm{top}} = 1.08 \pm 0.02(\mathrm{stat})$$

$$(\alpha^{1b}_{\mathrm{data}}/\alpha^{1b}_{\mathrm{MC}})^2 = 1.006$$

Top background (2)

- **For $N_j = 1$: normalized using CR ($N_b = 1$)**
  - In order to reduce large b-tagging uncertainties, the b-tagging efficiency is estimated from data (ε_{1j})

$$B^{\text{est}}_{\text{top},1j} = N_{\text{CR}} \cdot \underbrace{\left(\frac{1-\epsilon^{\text{est}}_{1j}}{\epsilon^{\text{est}}_{1j}}\right)}_{\alpha^{1j}_{\text{data}}}.$$

- Resulting NF:

$$\beta^{1j}_{\text{top}} = 1.06 \pm 0.03(\text{stat})$$

- Theory uncert. on extrapolation procedure:

Regions		Scale	PDF	Gen	UE/PS	Total
(b) $n_j = 1$. See the caption of Table XII for column headings.						
Signal region						
$e\mu$	$(10 < m_{\ell\ell} < 55)$	−1.1	−0.12	−2.4	2.4	3.6
$ee/\mu\mu$	$(12 < m_{\ell\ell} < 55)$	−1.0	−0.12	−2.0	3.0	3.7
WW control region						
$e\mu$	$(m_{\ell\ell} > 80)$	0.6	0.08	2.0	1.8	2.8

} Extrapolation factor from Top CR → SR

} Extrapolation factor from Top CR → WW CR

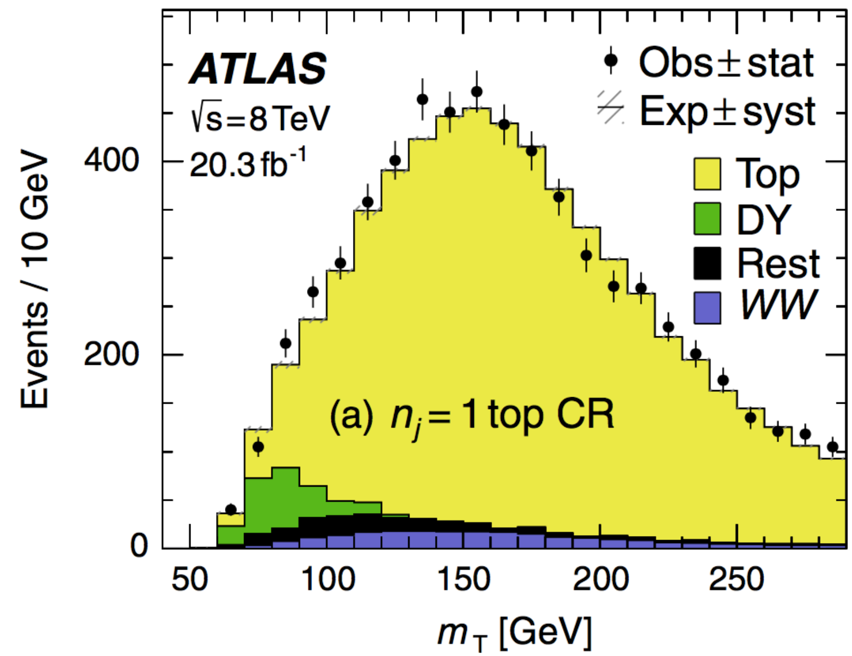

Top background (3)

- **For $N_j > 2$ (VBF-enriched): normalized using CR ($N_b = 1$)**
  - 1 b-jet CR mimcs top in SR (light-quark jet from ISR, and misidentified b-jet)
  - normalization (β) and extrapolation (α) factors evaluated for each BDT bin
  - Uncertainties below:

O_{BDT} bins	$\Delta\alpha/\alpha$	$\Delta\beta$ statistical	$\Delta\beta$ systematic	β
SR bin 0 (unused)	0.04	0.02	0.05	1.09
SR bin 1	0.10	0.15	0.55	1.58
SR bin 2	0.12	0.31	0.36	0.95
SR bin 3	0.21	0.31	0.36	0.95

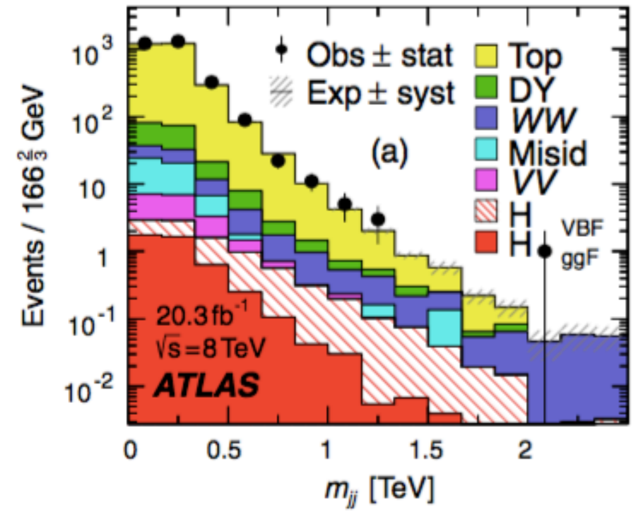

- **For $N_j > 2$ (ggF-enriched): normalized using CR ($N_b = 0$, $m_{ll} > 80$ GeV)**
  - To reduce b-tagging systematics CR defined instead for $N_b = 0$, with large m_{ll} (to keep orthogonal to SR and minimize signal)
  - Resulting NF: $$\beta = 1.05 \pm 0.03(\mathrm{stat})$$

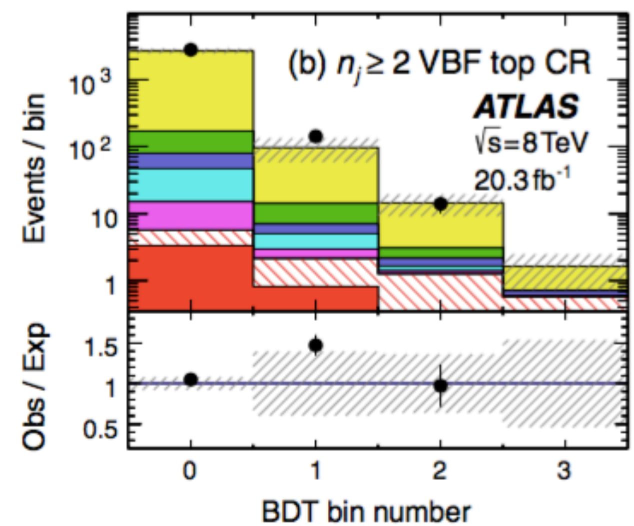

Misidentified leptons background

- W+jets (one mis-id lepton) or multijet (two mis-id lepton)
- Estimated using fake-factor method (data-driven)

$$N_{\text{one id, one fake}} = \frac{N_{\text{id obj}}}{N_{\text{anti-id}}} \times N_{\text{one id, one fakeable}}$$

fake factor

- Extrapolation factor ("fake factor") measured in data from Z+jets enriched region.
- Extrapolate to SR from a W+jets CR (both OS and SS)

SR p_T range	Total OC	Total SC	Corr. factor OC	Corr. factor SC	Stat	Other bkg
Electrons						
10–15 GeV	29	32	20	25	18	11
15–20 GeV	44	46	20	25	34	19
20–25 GeV	61	63	20	25	52	25
≥25 GeV	43	45	20	25	30	23
Muons						
10–15 GeV	25	37	22	35	10	03
15–20 GeV	37	46	22	35	18	05
20–25 GeV	37	46	22	35	29	09
≥25 GeV	46	53	22	35	34	21

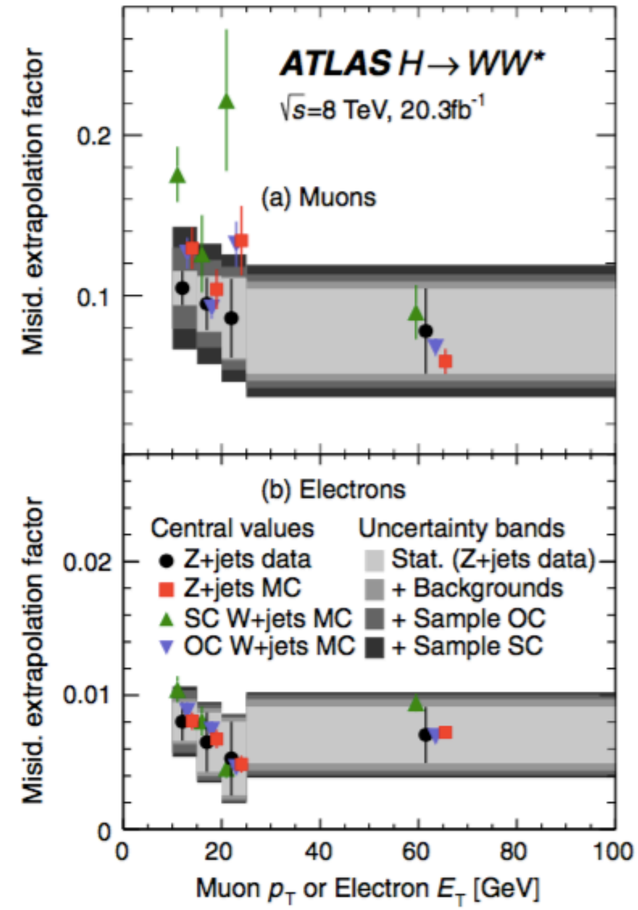

- Composition of associated jets (fraction of heavy flavour quark, light flavour quark, gluon initiated) may be different from Z+jets to W+jets sample.

Other diboson background

- ‘VV’ background include Wγ, Wγ^*, WZ and ZZ

- **<u>For eμ</u>**: one NF from data (same-sign CR) for all VV
- **<u>For ee/μμ</u>**: taken from simulation

- Wγ validated in region with reversed γ0conversion criteria
- Wγ^* validated in the 3-lepton region

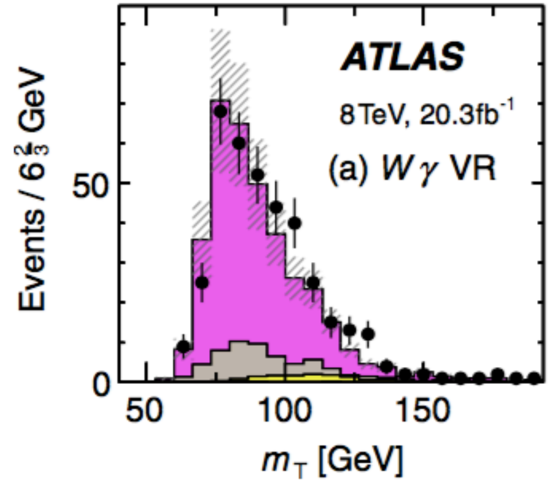

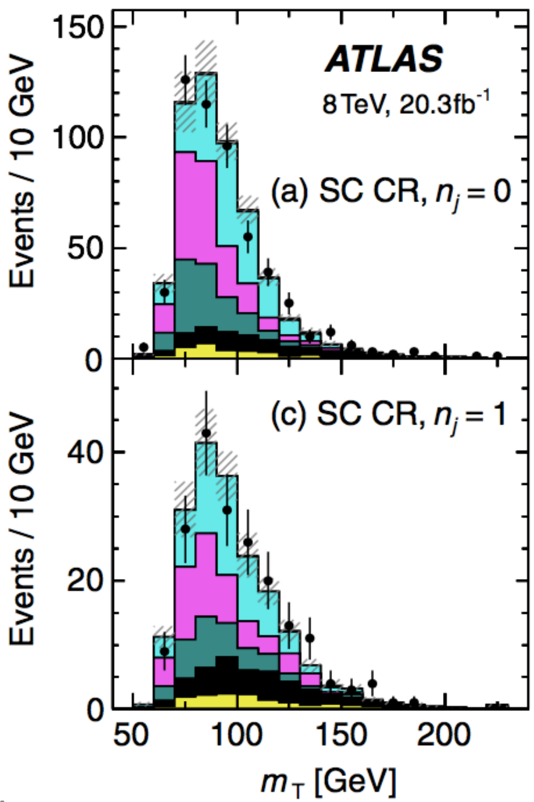

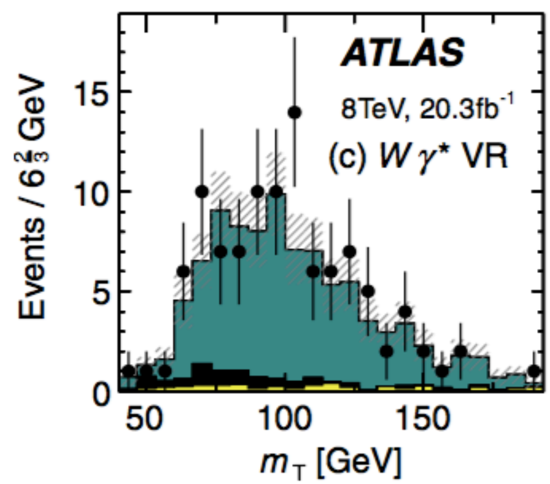

$$\beta_{0j} = 0.92 \pm 0.07(\text{stat})$$

$$\beta_{1j} = 0.96 \pm 0.12(\text{stat})$$

Z/DY background (1)

- **Z/DY→$\tau\tau$**
  - Normalization from CRs
  - 0j CR: eμ, m_{ll} < 80 GeV, $\Delta\phi_{ll}$ > 2.8
  - 1j CR: eμ, $m_{\tau\tau} > m_Z - 25$ GeV, m_{ll} < 80 GeV
  - 2j CR ggF: eμ, m_{ll} < 70 GeV, $\Delta\phi_{ll}$ > 2.8
  - 2j CR VBF: eμ(+ee+μμ), m_{ll} < 80 (75) GeV, $|m_{\tau\tau} - m_Z| < 25$ GeV

$$\beta_{0j} = 1.00 \pm 0.02(\text{stat})$$

$$\beta_{1j} = 1.05 \pm 0.04(\text{stat})$$

$$\beta_{2j} = 1.00 \pm 0.09(\text{stat})$$

$$\beta = 0.9 \pm 0.3(\text{stat})$$

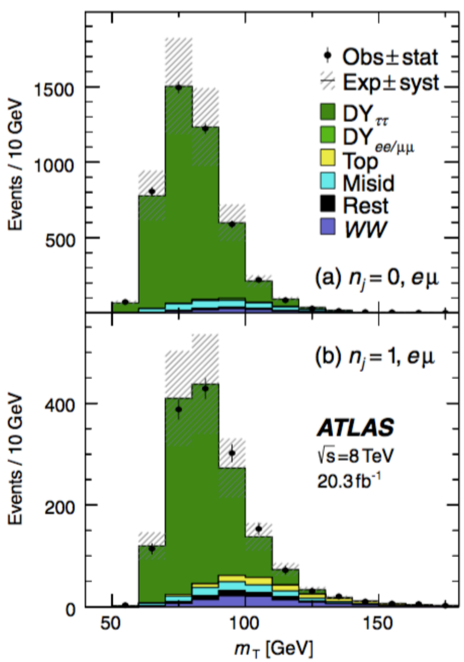

Regions	Scale	PDF	Gen	p_T^{Z/γ^*}
Signal regions				
$n_j = 0$	−1.6	1.4	5.7	19
$n_j = 1$	4.7	1.8	−2.0	-
$n_j \geq 2$ ggF	−10.3	1.1	10.4	-
WW control regions				
$n_j = 0$	−5.5	1.0	−8.0	16
$n_j = 1$	−7.2	2.1	3.2	-

Z/DY background (2)

- **Z/DY→ee/μμ in 0/1j:**
  - Data-driven via so-called "Pacman" method
  - f_{recoil} has clear shape difference with signal and Z/DY→$\tau\tau$
  - Method is based on measurement of selection efficiency of cut on f_{recoil} from data, and then estimating the remaining DY→ee/μμ after such a cut

$$\varepsilon = N_{\text{pass}}/(N_{\text{pass}} + N_{\text{fail}})$$

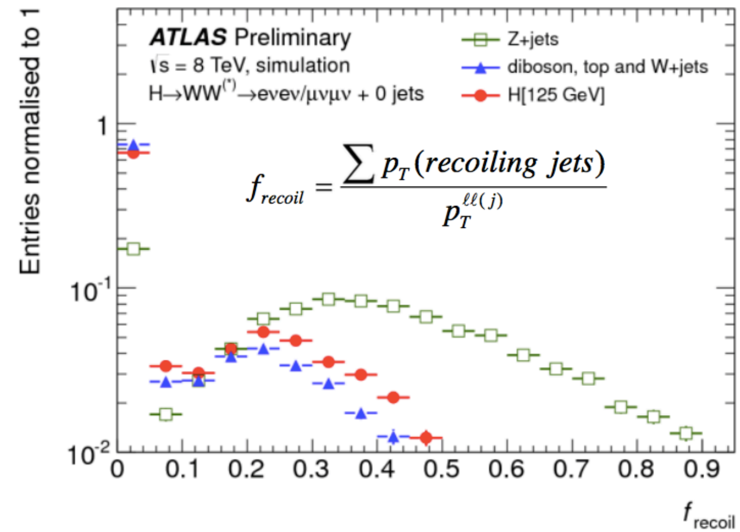

  - Analytically equivalent to inverting the matrix:

$$\begin{bmatrix} N_{\text{pass}} \\ N_{\text{pass}} + N_{\text{fail}} \end{bmatrix} = \begin{bmatrix} 1 & 1 \\ 1/\varepsilon_{\text{DY}} & 1/\varepsilon_{\text{non-DY}} \end{bmatrix} \cdot \begin{bmatrix} B_{\text{DY}} \\ B_{\text{non-DY}} \end{bmatrix}$$

  - ε_{DY} mesured in the ee/μμ sample, while $\varepsilon_{non\text{-}DY}$ measured in eμ sample that followins the selections of the ee/μμ analysis
  - Solving for B_{DY} gives the fully data-driven yield for DY→ee/μμ in the SR

- **Z/DY→ee/μμ in 2 jet:**
  - Data-driven ABCD method
  - A, B, C and D regions defined in MET-m_{ll} plane

VH Control Regions

Channel	4ℓ	3ℓ				
CR	ZZ	WZ	ZZ	Zjets	Top	$Z\gamma$
Number of leptons	4	3	3	3	3	3
Total lepton charge	0	±1	±1	±1	±1	±1
Number of SFOS	2	2 or 1	2 or 1	2 or 1	2 or 1	2 or 1
			($ee\mu$ or $\mu\mu\mu$)			($\mu\mu e$ or eee)
Number of jets	≤ 1	≤ 1	≤ 1	≤ 1	≥ 1	≤ 1
Number of b-jets	0	0	0	0	$\geq \mathbf{1}$	0
$E_{\mathrm{T}}^{\mathrm{miss}}$ (and/or) $p_{\mathrm{T}}^{\mathrm{miss}}$ [GeV]	—	> 30 and > 20	$< \mathbf{30}$ **or** $< \mathbf{20}$	$< \mathbf{30}$ **and** $< \mathbf{20}$	> 30 and > 20	$< \mathbf{30}$ **or** $< \mathbf{20}$
$\lvert m_{\ell\ell} - m_Z \rvert$ [GeV]	$< 10 (m_{\ell_2\ell_3})$	$< \mathbf{25}$	—	$< \mathbf{25}$	> 25	—
$\lvert m_{\ell\ell\ell} - m_Z \rvert$ [GeV]	—	—	< 15	> 15	—	$< \mathbf{15}$
Min. $m_{\ell\ell}$ [GeV]	$> \mathbf{65} (m_{\ell_0\ell_1})$	> 12	> 12	> 12	> 12	> 12
Max. $m_{\ell\ell}$ [GeV]	—	< 200	< 200	< 200	—	< 200
$\Delta R_{\ell_0\ell_1}$	—	< 2.0	< 2.0	< 2.0	—	< 2.0

Table 5. Definition of control regions in the 4ℓ and 3ℓ analyses. Selections indicated in boldface font are designed to retain the CR orthogonal to the relevant SR.

VH NFs and CRs

(a) 8 TeV data sample

Channel	4ℓ	3ℓ
Category	2SFOS, 1SFOS	3SF, 1SFOS, 0SFOS
Process		
$WZ/W\gamma^*$	—	$1.08^{+0.08}_{-0.06}$
ZZ^*	$1.03^{+0.11}_{-0.10}$	$1.28^{+0.22}_{-0.20}$
OS WW	—	—
$W\gamma$	—	—
$Z\gamma$	—	$0.62^{+0.15}_{-0.14}$
Z/γ^*	—	$0.80^{+0.68}_{-0.53}$ (μ-misid)
		$0.33^{+0.12}_{-0.11}$ (e-misid)
Top	—	$1.36^{+0.34}_{-0.30}$

3lep CRs

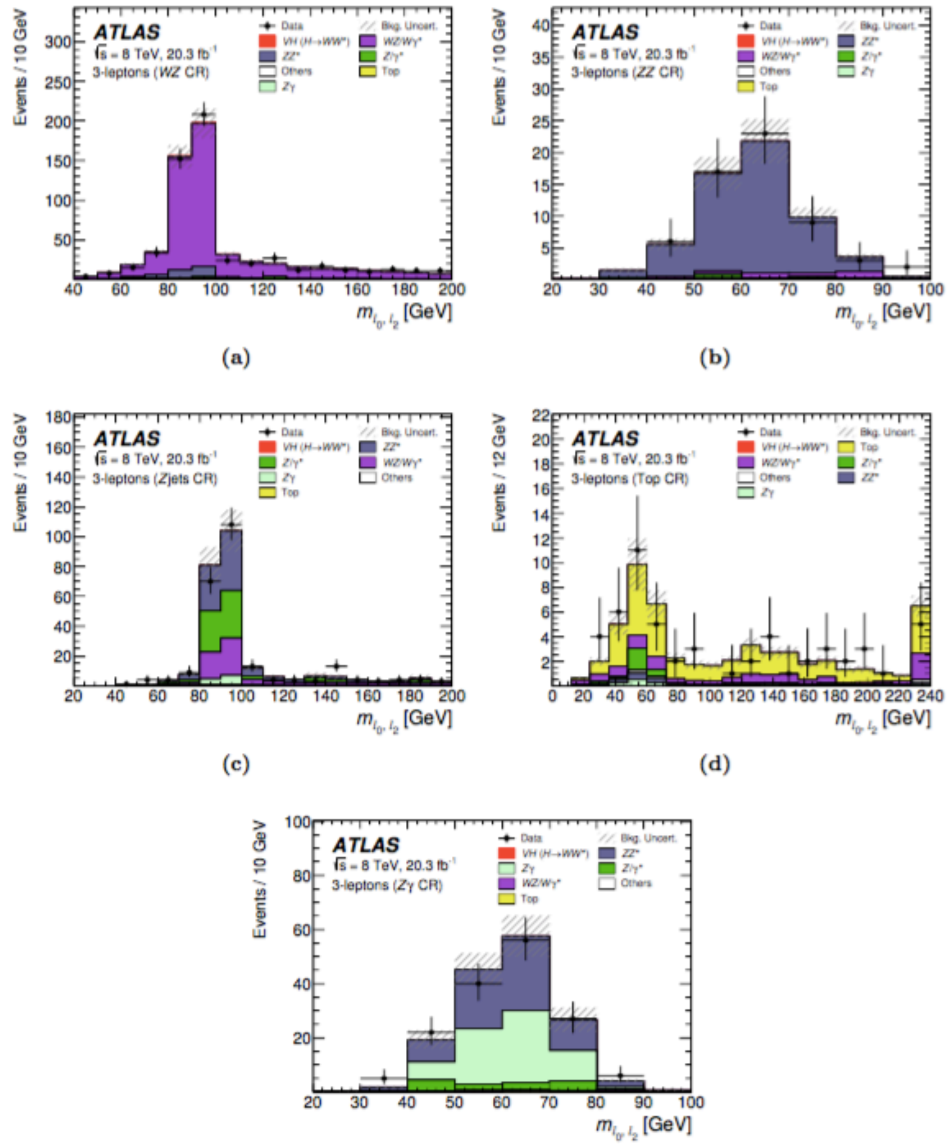

4lep ZZ CR

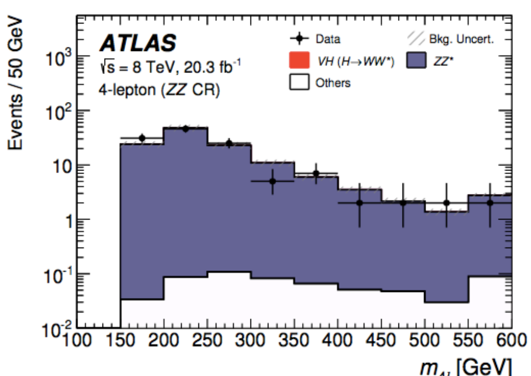

Signal theory uncertainties

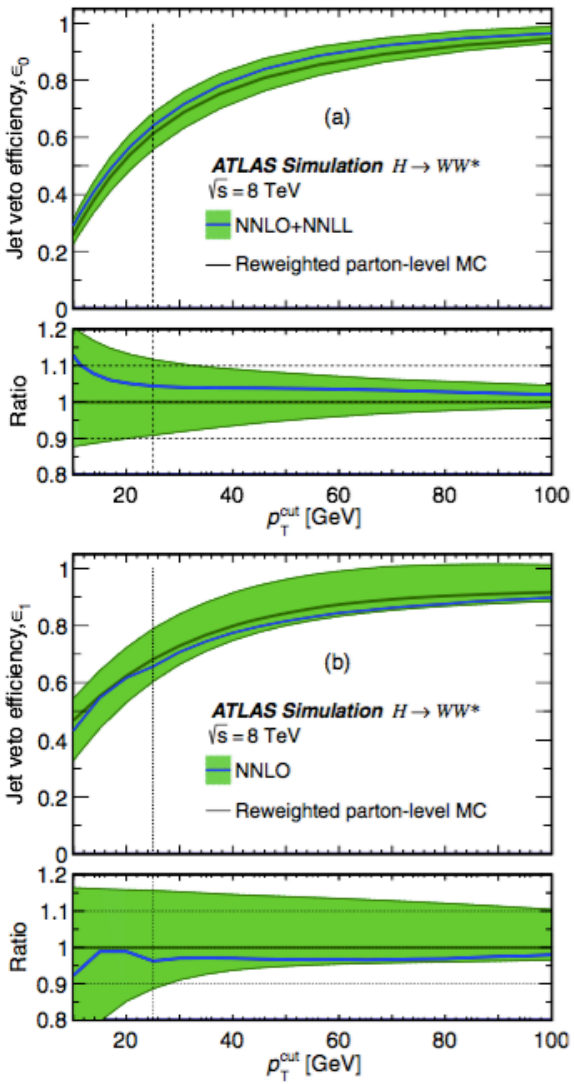

FIG. 18 (color online). Efficiencies of the veto of the (a) first jet and (b) second jet in inclusive ggF production of the Higgs boson, as a function of the veto-threshold p_T.

TABLE X. Signal-yield uncertainties (in %) due to the modeling of the gluon-fusion and vector-boson-fusion processes. For the $n_j = 0$ and $n_j = 1$ categories the uncertainties are shown for events with same-flavor leptons; for events with different-flavor leptons the uncertainties are evaluated in bins of $m_{\ell\ell}$ and $p_T^{\ell 2}$. For the $n_j \geq 2$ VBF category the uncertainties are shown for the most sensitive bin of BDT output (bin 3).

Uncertainty source	$n_j = 0$	$n_j = 1$	$n_j \geq 2$ ggF	$n_j \geq 2$ VBF
Gluon fusion				
Total cross section	10	10	10	7.2
Jet binning or veto	11	25	33	29
Acceptance				
Scale	1.4	1.9	3.6	48
PDF	3.2	2.8	2.2	-
Generator	2.5	1.4	4.5	-
UE/PS	6.4	2.1	1.7	15
Vector-boson fusion				
Total cross section	2.7	2.7	2.7	2.7
Acceptance				
Scale	-	-	-	3.0
PDF	-	-	-	3.0
Generator	-	-	-	4.2
UE/PS	-	-	-	14

Systematic uncertainties: signal

TABLE XXII. Sources of systematic uncertainty (in %) on the predicted signal yield (N_{sig}) and the cumulative background yields (N_{bkg}). Entries marked with a dash (-) indicate that the corresponding uncertainties either do not apply or are less than 0.1%. The values are postfit and given for the 8 TeV analysis.

	$n_j = 0$	$n_j = 1$	$n_j \geq 2$ ggF	$n_j \geq 2$ VBF
(a) Uncertainties on N_{sig} (in %)				
ggF H, jet veto for $n_j = 0$, ϵ_0	8.1	14	12	-
ggF H, jet veto for $n_j = 1$, ϵ_1	-	12	15	-
ggF H, $n_j \geq 2$ cross section	-	-	-	6.9
ggF H, $n_j \geq 3$ cross section	-	-	-	3.1
ggF H, total cross section	10	9.1	7.9	2.0
ggF H acceptance model	4.8	4.5	4.2	4.0
VBF H, total cross section	-	0.4	0.8	2.9
VBF H acceptance model	-	0.3	0.6	5.5
$H \to WW^*$ branching fraction	4.3	4.3	4.3	4.3
Integrated luminosity	2.8	2.8	2.8	2.8
Jet energy scale & resolution	5.1	2.3	7.1	5.4
p_T^{miss} scale & resolution	0.6	1.4	0.1	1.2
f_{recoil} efficiency	2.5	2.1	-	-
Trigger efficiency	0.8	0.7	-	0.4
Electron id., isolation, reconstruction eff.	1.4	1.6	1.2	1.0
Muon id., isolation, reconstruction eff.	1.1	1.6	0.8	0.9
Pile-up model	1.2	0.8	0.8	1.7

- Dominant uncertainties on the signal yield are theoretical
- Dominant experimental uncertainties are jet energy scale and resolution, and b-tagging efficiency.

Systematic uncertainties: bkg

	$n_j = 0$	$n_j = 1$	$n_j \geq 2$ ggF	$n_j \geq 2$ VBF
(b) Uncertainties on $N_{\rm bkg}$ (in %)				
WW theoretical model	1.4	1.6	0.7	3.0
Top theoretical model	-	1.2	1.7	3.0
VV theoretical model	-	0.4	1.1	0.5
$Z/\gamma^* \to \tau\tau$ estimate	0.6	0.3	1.6	1.6
$Z/\gamma^* \to ee, \mu\mu$ estimate in VBF	-	-	-	4.8
Wj estimate	1.0	0.8	1.6	1.3
jj estimate	0.1	0.1	1.8	0.9
Integrated luminosity	-	-	0.1	0.4
Jet energy scale & resolution	0.4	0.7	0.9	2.7
$p_{\rm T}^{\rm miss}$ scale & resolution	0.1	0.3	0.5	1.6
b-tagging efficiency	-	0.2	0.4	2.0
Light- and c-jet mistag	-	0.2	0.4	2.0
$f_{\rm recoil}$ efficiency	0.5	0.5	-	-
Trigger efficiency	0.3	0.3	0.1	-
Electron id., isolation, reconstruction eff.	0.3	0.3	0.2	0.3
Muon id., isolation, reconstruction eff.	0.2	0.2	0.3	0.2
Pile-up model	0.4	0.5	0.2	0.8

- Dominant experimental uncertainties are jet energy scale and resolution, and b-tagging efficiency.

Systematic uncertainties: *VH* channels

(a) Uncertainties on the $VH(H \to WW^*)$ process (%)

Channel	4ℓ		3ℓ			2ℓ		
Category	2SFOS	1SFOS	3SF	1SFOS	0SFOS	DFOS	SS2jet	SS1jet
Theoretical uncertainties								
VH acceptance	9.2	9.3	9.9	9.9	9.9	10	10	9.9
Higgs boson branching fraction	4.2	4.2	4.2	4.2	4.2	4.2	4.2	4.2
QCD scale	3.1	3.0	1.2	1.0	1.0	1.3	1.0	1.0
PDF and α_S	1.0	1.1	2.1	2.2	2.2	1.9	2.3	2.2
VH NLO EW corrections	1.7	1.8	1.9	1.9	1.9	1.9	1.9	1.9
Experimental uncertainties								
Jet	2.0	3.1	2.5	2.5	2.9	3.2	8.9	5.8
E_T^{miss} soft term	0.2	0.3	—	—	—	0.3	0.6	0.2
Electron	2.6	2.8	1.6	2.2	2.2	1.5	2.1	1.7
Muon	2.6	2.4	2.2	1.8	1.7	0.8	1.8	1.9
Trigger efficiency	0.2	—	0.4	0.3	0.3	0.5	0.6	0.5
b-tagging efficiency	0.9	0.9	0.9	0.8	0.8	2.9	3.5	2.4
Pile-up	1.9	0.7	2.0	1.4	0.8	1.7	1.0	2.4
Luminosity	2.8	2.8	2.8	2.8	2.8	2.8	2.8	2.8

(b) Uncertainties on the total background (%)

Theoretical uncertainties								
QCD scale	0.2	0.1	1.0	0.9	—	3.7	13	2.3
PDF and α_S	0.2	2.4	0.3	0.3	1.6	1.4	0.5	0.6
VVV K-factor	2.8	8.1	1.1	1.9	0.5	—	—	0.3
MC modelling	5.3	4.3	7.0	6.6	—	4.1	0.8	1.4
Experimental uncertainties								
Jet	3.1	2.4	3.2	1.8	4.1	7.2	5.0	3.4
E_T^{miss} soft term	2.3	0.6	1.8	1.9	0.5	1.1	0.2	0.7
Electron	1.0	1.4	1.0	0.4	1.1	0.7	1.1	0.8
Muon	1.1	1.2	0.4	0.7	0.2	0.2	0.4	0.8
Trigger efficiency	—	0.2	0.2	—	—	0.1	—	—
b-tagging efficiency	0.6	0.8	0.6	0.8	2.6	0.7	1.4	0.3
Fake factor	—	—	—	—	—	2.8	10	10
Charge mis-assignment	—	—	—	—	1.4	—	0.7	0.8
Photon conversion rate	—	—	—	—	—	—	1.1	0.9
Pile-up	1.2	1.1	1.4	0.3	1.2	0.9	1.0	1.0
Luminosity	0.4	0.8	0.1	0.2	0.7	—	0.7	0.3
MC statistics	5.3	8.0	3.8	3.2	5.5	3.1	7.3	3.9
CR statistics	8.1	6.6	4.2	3.9	8.8	2.5	2.8	3.5

Table 9. Theoretical and experimental uncertainties, in %, on the predictions of the (a) signal and (b) total background for each category. Fake factor refers to the data-driven estimates of the W+jets and multijet backgrounds in the 2ℓ channels. The dash symbol (–) indicates that the corresponding uncertainties either do not apply or are negligible. The values are obtained through the fit and given for the 8 TeV data sample. Similar values are obtained for the 7 TeV data sample.

Fit procedure (1)

- Regions that enter the fit:

  1. **Signal regions catagories**
     - 7 and 8 TeV
     - N_j = 0, 1, and $\geq$2 jets VBF/ggF
     - ee, μμ, eμ, μe
     - m_{ll} slices (typically 1 or 2 depending on category)
     - p_T^{l2} slices (typically 1, 2 or 3 depending on category)

  2. **Control regions**
     - See next slide for exact profiled regions / non-profiled regions
     - Profiled CRs determine the normalization of corresponding backgrounds through Poisson term in the likelihood
     - Nonprofieled CRs do not have explicit termins in the likelihood, and enter the fit in other ways

- Fit variables are m_T in the ggF-enriched categories, and BDT output in VBF-enriched category.

- Exact binning schemes in above two variables chosen to maximize expected significance while stabilizing the stat fluctuations associated to subtraction of backgrounds.

Fit procedure (2)

CR	Profiled?	Sample	Notable differences vs. SR
(b) Control regions that are profiled (•) and nonprofiled (∘)			
$n_j = 0$			
WW	•	$e\mu$	$55 < m_{\ell\ell} < 110$, $\Delta\phi_{\ell\ell} < 2.6$, $p_{\mathrm{T}}^{\ell 2} > 15$
Top	∘	$e\mu$	$n_j = 0$ after presel., $\Delta\phi_{\ell\ell} < 2.8$
Wj	∘	same	one anti-identified ℓ
jj	∘	same	two anti-identified ℓ
VV	•	$e\mu$	same-charge ℓ (only used in $e\mu$)
DY, $ee/\mu\mu$	•	$ee/\mu\mu$	$f_{\mathrm{recoil}} > 0.1$ (only used in $ee/\mu\mu$)
DY, $\tau\tau$	•	$e\mu$	$m_{\ell\ell} < 80$, $\Delta\phi_{\ell\ell} > 2.8$
$n_j = 1$			
WW	•	$e\mu$	$m_{\ell\ell} > 80$, $\lvert m_{\tau\tau} - m_Z\rvert > 25$, $p_{\mathrm{T}}^{\ell 2} > 15$
Top	•	$e\mu$	$n_b = 1$
Wj	∘	same	one anti-identified ℓ
jj	∘	same	two anti-identified ℓ
VV	•	$e\mu$	same-charge ℓ (only used in $e\mu$)
DY, $ee/\mu\mu$	•	$ee/\mu\mu$	$f_{\mathrm{recoil}} > 0.1$ (only used in $ee/\mu\mu$)
DY, $\tau\tau$	•	$e\mu$	$m_{\ell\ell} < 80$, $m_{\tau\tau} > m_Z - 25$
$n_j \geq 2$ ggF			
Top	•	$e\mu$	$m_{\ell\ell} > 80$
Wj	∘	same	one anti-identified ℓ
jj	∘	same	two anti-identified ℓ
DY, $\tau\tau$	•	$e\mu$	$m_{\ell\ell} < 70$, $\Delta\phi_{\ell\ell} > 2.8$
$n_j \geq 2$ VBF			
Top	•	both	$n_b = 1$
Wj	∘	same	one anti-identified ℓ
jj	∘	same	two anti-identified ℓ
DY, $ee/\mu\mu$	∘	$ee/\mu\mu$	$E_{\mathrm{T}}^{\mathrm{miss}} < 45$ (only used in $ee/\mu\mu$)
DY, $\tau\tau$	∘	both	$m_{\ell\ell} < 80$, $\lvert m_{\tau\tau} - m_Z\rvert < 25$

Fit procedure (3)

- Likelihood function is defined to simultaneously model or 'fit' the yields of the various subsample, and is maximized

$$\mathcal{L} = \underbrace{\prod_{i,b}^{\substack{\text{Table}\\ \text{XXIa}}} f\left(N_{ib} \,\middle|\, \mu \cdot S_{ib} \prod_{r}^{\substack{\text{Syst in}\\ \text{Sec. V}}} v_{br}(\theta_r) + \sum_{k}^{\substack{\text{Table}\\ \text{I}}} \beta_k \cdot B_{kib} \prod_{s}^{\substack{\text{Syst in}\\ \text{Sec. VII C}}} v_{bs}(\theta_s)\right)}_{\text{Poisson for SR with signal strength } \mu\text{; predictions } S,\, B} \underbrace{\prod_{l}^{\substack{\text{Table}\\ \text{XXIb}\bullet}} f\left(N_l \,\middle|\, \sum_{k}^{\substack{\text{Table}\\ \text{I}}} \beta_k \cdot B_{kl}\right)}_{\text{Poisson for profiled CRs}} \underbrace{\prod_{t}^{\substack{\text{Syst in}\\ \{r,s\}}} g(\vartheta_t \,|\, \theta_t)}_{\text{Gauss. for syst}} \underbrace{\prod_{k}^{\substack{\text{Table}\\ \text{I}}} f(\xi_k \,|\, \zeta_k \cdot \theta_k)}_{\text{Poiss. for MC stats}}.$$

- Profile likelihood-ratio test statistics used to test the background-only or background-and-signal hypothesis

$$q(\mu) = -2\ln \frac{\mathcal{L}(\mu, \boldsymbol{\theta})}{\mathcal{L}_{\max}}\bigg|_{\boldsymbol{\theta}=\hat{\boldsymbol{\theta}}_{\mu}},$$

3. Combined fit

The combined results for the 7 and 8 TeV data samples account for the correlations between the analyses due to common systematic uncertainties.

The correlation of all respective nuisance parameters is assumed to be 100% except for those that are statistical in origin or have a different source for the two data sets. Uncorrelated systematics include the statistical component of the jet energy scale calibration and the luminosity uncertainty. All theoretical uncertainties are treated as correlated.

Impact of nuisance parameters on μ

TABLE XXIV. Impact on the signal strength $\hat{\mu}$ from the prefit and postfit variations of the nuisance parameter uncertainties, Δ_θ. The + (−) column header indicates the positive (negative) variation of Δ_θ and the resulting change in $\hat{\mu}$ is noted in the entry (the sign represents the direction of the change). The right-hand side shows the pull of θ and the data constraint of Δ_θ. The pulls are given in units of standard deviations (σ) and Δ_θ of ± 1 means no data constraint. The rows are ordered by the size of a change in $\hat{\mu}$ due to varying θ by the postfit uncertainty Δ_θ.

Systematic source	Impact on $\hat{\mu}$: Prefit $\Delta_{\hat{\mu}}$ +	Prefit $\Delta_{\hat{\mu}}$ −	Postfit $\Delta_{\hat{\mu}}$ +	Postfit $\Delta_{\hat{\mu}}$ −	Plot of postfit $\pm\Delta_{\hat{\mu}}$	Impact on $\hat{\theta}$: Pull, $\hat{\theta}$ (σ)	Constraint, Δ_θ
ggF H, PDF variations on cross section	−0.06	+0.06	−0.06	+0.06		−0.06	±1
ggF H, QCD scale on total cross section	−0.05	+0.06	−0.05	+0.06		−0.05	±1
WW, generator modeling	−0.07	+0.06	−0.05	+0.05		0	±0.7
Top quarks, generator modeling on α_{top} in ggF cat.	+0.03	−0.03	+0.03	−0.03		−0.40	±0.9
Misid of μ, OC uncorrelated corr factor α_{misid}, 2012	−0.03	+0.03	−0.03	+0.03		0.48	±0.8
Integrated luminosity, 2012	−0.03	+0.03	−0.03	+0.03		0.08	±1
Misid of e, OC uncorrelated corr factor α_{misid}, 2012	−0.03	+0.03	−0.02	+0.03		−0.06	±0.9
ggF H, PDF variations on acceptance	−0.02	+0.02	−0.02	+0.02		−0.03	±1
Jet energy scale, η intercalibration	−0.02	+0.02	−0.02	+0.02		0.45	±0.95
VBF H, UE/PS	−0.02	+0.02	−0.02	+0.02		0.26	±1
ggF H, QCD scale on ϵ_1	−0.01	+0.03	−0.01	+0.03		−0.10	±0.95
Muon isolation efficiency	−0.02	+0.02	−0.02	+0.02		0.13	±1
VV, QCD scale on acceptance	−0.02	+0.02	−0.02	+0.02		0.09	±1
ggF H, UE/PS	-	−0.02	-	−0.02		0	±0.9
ggF H, QCD scale on acceptance	−0.02	+0.02	−0.02	+0.02		0	±1
Light jets, tagging efficiency	+0.02	−0.02	+0.02	−0.02		0.21	±1
ggF H, generator modeling on acceptance	+0.01	−0.02	+0.01	−0.02		0.10	±1
ggF H, QCD scale on $n_j \geq 2$ cross section	−0.01	+0.02	−0.01	+0.02		−0.04	±1
Top quarks, generator modeling on α_{top} in VBF cat.	−0.01	+0.02	−0.01	+0.02		−0.16	±1
Electron isolation efficiency	−0.02	+0.02	−0.02	+0.02		−0.14	±1

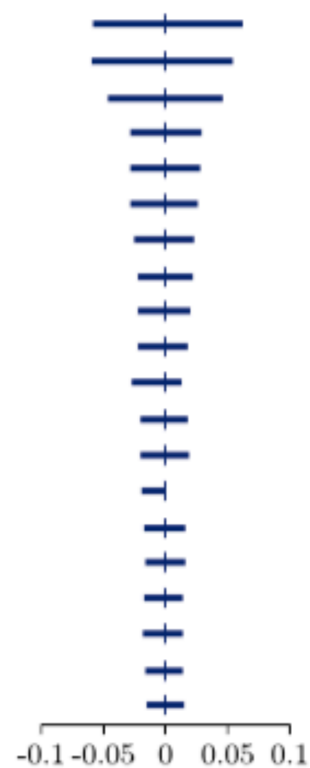

Impact on μ: *VH* channels

Uncertainties on the signal strength μ_{VH} (%)

Signal theoretical uncertainties	$\Delta\mu_{VH}/\mu_{VH}$	
	+	-
VH acceptance	11	7
Higgs boson branching fraction	7	4
QCD scale	1.6	0.7
PDF and α_S	3.2	1.5
VH NLO EW corrections	2.5	1.2
Background theoretical uncertainties		
QCD scale	10	9
PDF and α_S	2.3	2.0
VVV K-factor	3.0	3.0
MC modelling	7.5	6.9
Experimental uncertainties		
Jet	14	9
E_T^{miss} soft term	3.4	2.3
Electron	4.8	2.9
Muon	4.8	3.2
Trigger efficiency	1.7	0.9
b-tagging efficiency	4.7	3.2
Fake factor	14	12
Charge mis-assignment	1.1	1.0
Photon conversion rate	0.8	0.7
Pile-up	3.0	1.9
Luminosity	5.4	3.3
MC statistics	8	8
CR statistics	18	15
ggF SR statistics	5.5	4.4
VBF SR statistics	1.9	1.5
ggF+VBF CR statistics	10	9

Table 14. Percentage theoretical and experimental uncertainties on the observed VH signal strength μ_{VH}. The contributions from signal-related and background-related theoretical uncertainties are specified. The "VH acceptance" is evaluated using both the $qq \to (W/Z)H$ and the $gg \to ZH$ production. The statistical uncertainty due to the ggF and VBF subtraction measured in the categories of the ggF and VBF analysis are indicated with "ggF SR statistics" and "VBF SR statistics", for the contribution from the signal regions, and "ggF+VBF CR statistics" for the contribution from the control regions. The row "MC statistics" shows the uncertainty due to the statistics of the simulated samples. The values are obtained from the combination of the 8 TeV and 7 TeV data samples.

Significance and μ measurements

Category	Signal significance Z_0			Observed signal strength μ					
	Exp. Z_0	Obs. Z_0	Obs. Z_0	μ	Tot. err. +	Tot. err. −	Syst. err. +	Syst. err. −	μ
ggF	4.4	4.2		0.98	0.29	0.26	0.22	0.18	
VBF	2.6	3.2		1.28	0.55	0.47	0.32	0.25	
VH	0.93	2.5		3.0	1.6	1.3	0.95	0.65	
WH only	0.77	1.4		2.1	1.9	1.6	1.2	0.79	
ZH only	0.30	2.0		5.1	4.3	3.1	1.9	0.89	
ggF+VBF+VH	5.9	6.5		1.16	0.24	0.21	0.18	0.15	
			0 1 2 3 4 5 6 7						0 1 2 3 4 5 6 7 8 9 10

Significance and μ: *VH* channels

Category	Signal significance Z_0 Exp. Z_0	Obs. Z_0	Observed signal strength μ: μ	Tot. err. +	Tot. err. −	Syst. err. +	Syst. err. −
4ℓ	0.41	1.9	4.9	4.6	3.1	1.1	0.40
2SFOS	0.19	0	−5.9	6.8	4.1	0.33	0.72
1SFOS	0.36	2.5	9.6	8.1	5.4	2.1	0.64
3ℓ	0.79	0.66	0.72	1.3	1.1	0.40	0.29
1SFOS and 3SF	0.41	0	−2.9	2.7	2.1	1.2	0.92
0SFOS	0.68	1.2	1.7	1.9	1.4	0.51	0.29
2ℓ	0.59	2.1	3.7	1.9	1.5	1.1	1.1
DFOS	0.54	1.2	2.2	2.0	1.9	1.0	1.1
SS2jet	0.17	1.4	7.6	6.0	5.4	3.2	3.2
SS1jet	0.27	2.3	8.4	4.3	3.8	2.3	2.0

Obs. Z_0

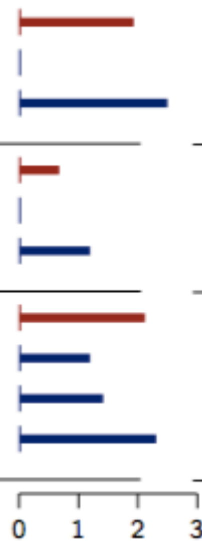

μ

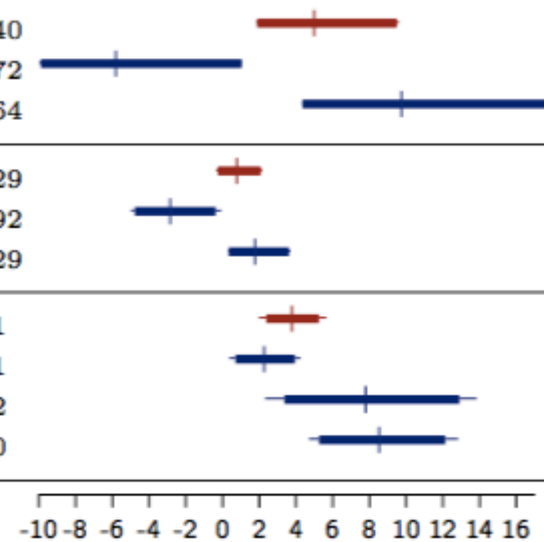

$$\mu_{WH} = 2.1^{+1.5}_{-1.3}\,(\text{stat.})^{+1.2}_{-0.8}\,(\text{sys.}),\qquad \mu_{ZH} = 5.1^{+3.8}_{-3.0}\,(\text{stat.})^{+1.9}_{-0.9}\,(\text{sys.}),$$

$$\mu_{VH} = 3.0^{+1.3}_{-1.1}\,(\text{stat.})^{+1.0}_{-0.7}\,(\text{sys.}).$$

Likelihood curves for signal strength

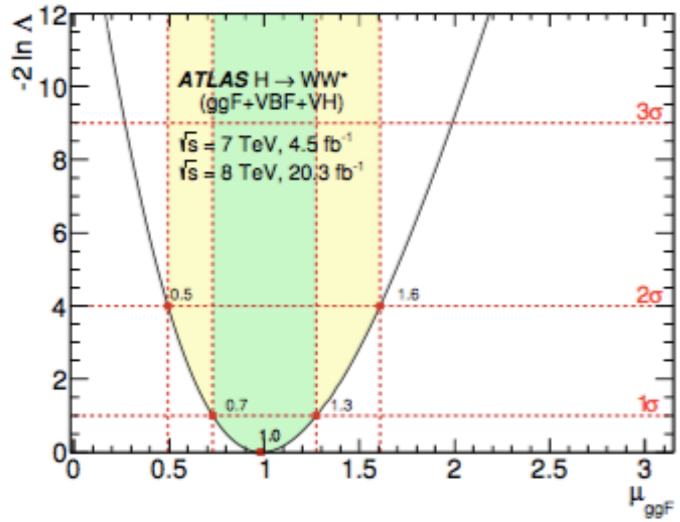

(a)

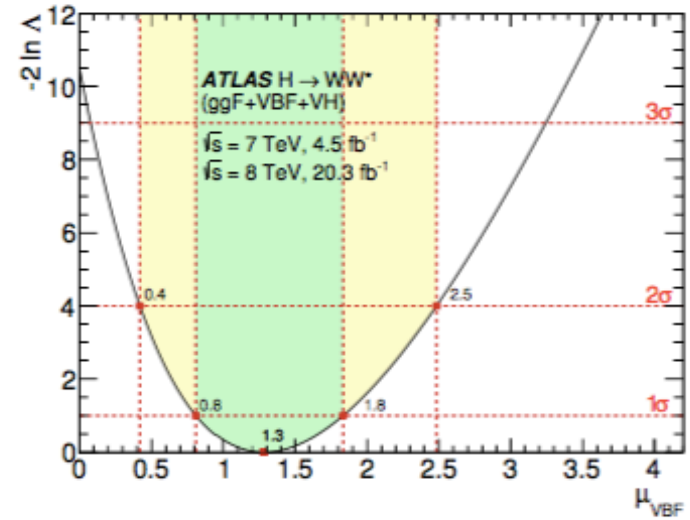

(b)

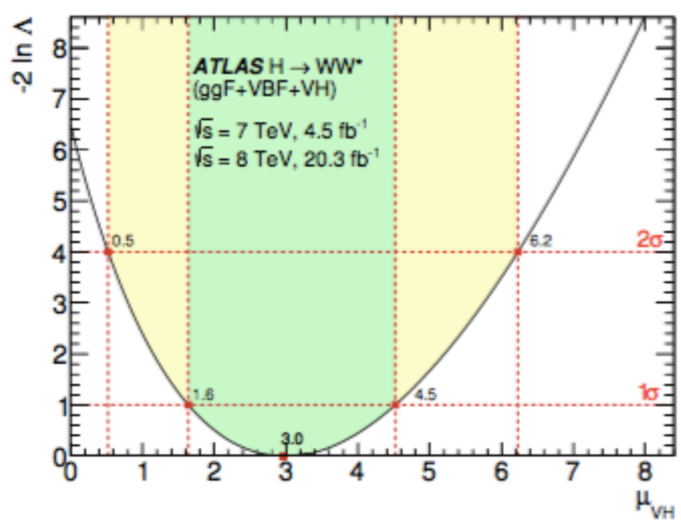

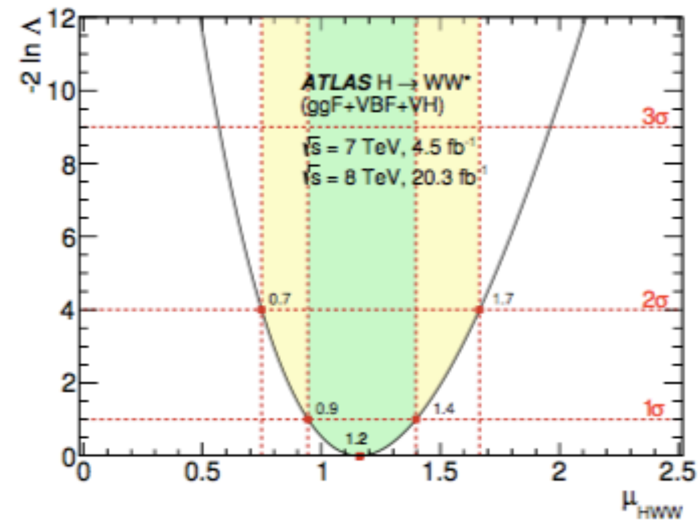

High-mass: object definitions

- Primary vertex (PV) = 1
  - ≥ 2 associated tracks with $p_T > 400$ MeV
  - if > 1 vertex meet the requirement above, the largest track $\sum p_T^2$ chosen as PV
- Electron
  - MediumLH for pT > 25 GeV or TightLH for 15 < pT < 25GeV
  - $|\eta| < 2.47$, except for $1.37 < |\eta| < 1.52$
- Muon
  - Medium for pT > 25 GeV or Tight for 15 < pT < 25GeV
  - $|\eta| < 2.5$
- Jet
  - $p_T > 30$ GeV, $|\eta| < 4.5$
  - JVT > 0.59 for $p_T < 60$ GeV
  - Overlap removal with electrons and muons
- B-tagged jet
  - Identified using the MV2c10 b-tagging algorithm, with an efficiency of 85%
  - $p_T > 20$ GeV, $|\eta| < 2.5$

High-mass: object definitions

- MET: missing transverse momentum
  - E_T^{miss}: calorimeter-based

    Negative vectorial sum of the transverse momenta of all calibrated selected objects

    Tracks compatible with the primary vertex but not matched to the objects also included
  - p_T^{miss}: track-based

    negative sum of the momenta of ID tracks, satisfying:
    - $d_0 < 1.5$mm, $d_0/\sigma(d_0) < 3$
    - $|\eta| < 2.5$, $p_T > 500$ MeV

    Calorimeter electron p_T used instead of track p_T

High-mass: transverse mass

- Transverse missing momentum:

  Negative vectorial sum of the transverse momenta

  - $\mathbf{E_T^{miss}}$: based on calorimeter objects
  - $\mathbf{p_T^{miss}}$: based on charged tracks

- Transverse invariant mass:

$$M_T = \sqrt{(E_T^{ll} + E_T^{miss})^2 - |\,\mathbf{p}_T^{ll} + \mathbf{E}_T^{miss}\,|^2}$$

→ Discriminating variable

$$where \quad E_T^{ll} = \sqrt{|\,\mathbf{p}_T^{ll}\,| + m_{ll}^2}$$

High-mass: event selection optimization

- Developed a simple and general optimization procedure
  1. Select the most discriminating variables from the BDT training

     Remove duplicated variables that highly correlated

  2. Choose cut values for each variable by maximizing the signal significance
- Scanning on leading lepton p_T

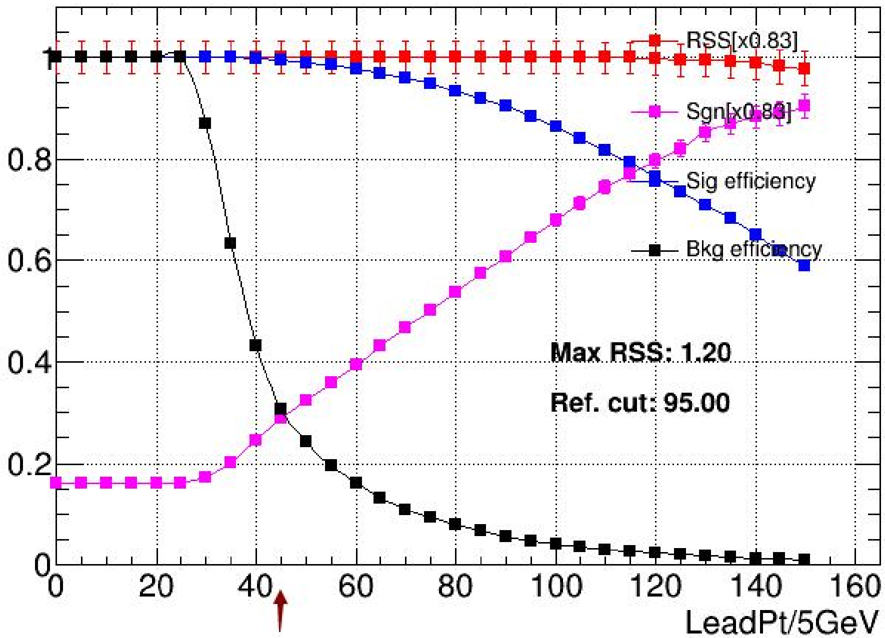

N-1 scanning: also other cuts applied

- Naming on this plot:

$$RSS = \sqrt{\sum_{i}^{N_{\text{bins}}} Sgn_i^2}$$

$$Sgn = \sqrt{2\left[(n_S + n_B)\ln\left(1 + \frac{n_S}{n_B}\right) - n_S\right]}$$

High-mass: SR event selections

- Event selection in signal regions(SRs) :
  - VBF 1J phase space: $N_{\text{jet}} = 1:\ |\eta_j| > 2.4 \text{ and } \min(|\Delta\eta_{j\ell}|) > 1.75$
  - VBF 2J phase space: $N_{\text{jet}} \geq 2:\ m_{jj} > 500 \text{ GeV and } |\Delta y_{jj}| > 4$

Preselection cuts: $p_{\mathrm{T}}^{\text{lead}} > 25$ GeV, $p_{\mathrm{T}}^{\text{sublead}} > 15$ GeV, 3rd lepton veto, $m_{\ell\ell} > 10$ GeV		
$\mathrm{SR}_{\mathrm{ggF}}$	$\mathrm{SR}_{\mathrm{VBF1J}}$	$\mathrm{SR}_{\mathrm{VBF2J}}$
$N_{b\text{-jet}} = 0$ $\lvert\Delta\eta_{\ell\ell}\rvert < 1.8$ $m_{\ell\ell} > 55$ GeV $p_{\mathrm{T}}^{\text{lead}} > 45$ GeV $p_{\mathrm{T}}^{\text{sublead}} > 30$ GeV $\max(m_{\mathrm{T}}^{W}) > 50$ GeV		
Inclusive in N_{jet} but excluding VBF1J and VBF2J phase space	$N_{\text{jet}} = 1$ $\lvert\eta_j\rvert > 2.4$ $\min(\lvert\Delta\eta_{j\ell}\rvert) > 1.75$	$N_{\text{jet}} \geq 2$ $m_{jj} > 500$ GeV $\lvert\Delta y_{jj}\rvert > 4$

$$m_{\mathrm{T}}^{W} = \sqrt{2 p_{\mathrm{T}}^{\ell} E_{\mathrm{T}}^{\text{miss}} (1 - \cos(\phi^{\ell} - \phi^{E_{\mathrm{T}}^{\text{miss}}}))}$$

High-mass: acceptance * efficiency

- Selection efficiency (not including pre-selection cuts)

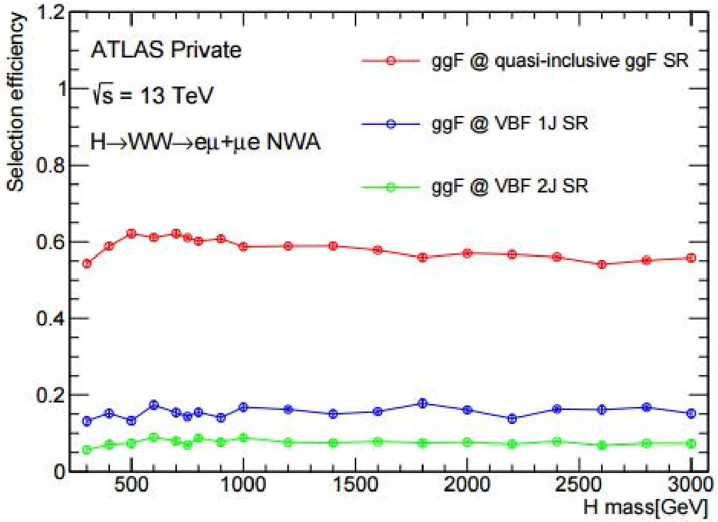

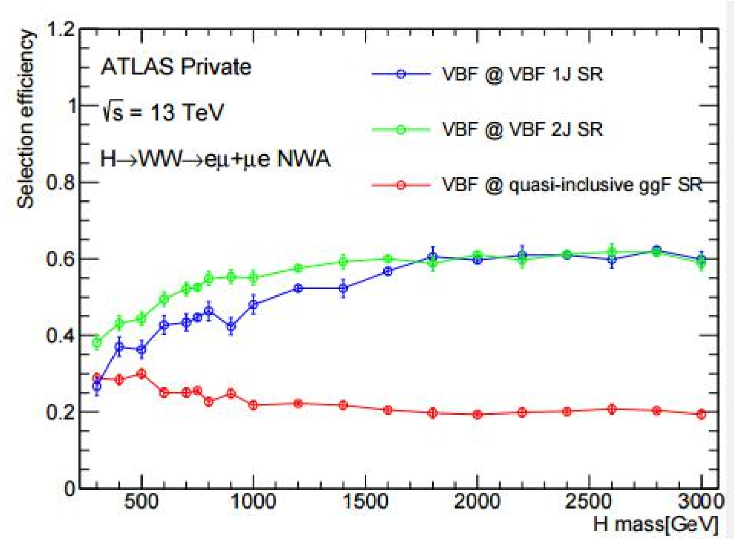

- Acceptane*efficiency (namely the <u>overall efficiency</u> after all selections in SR)

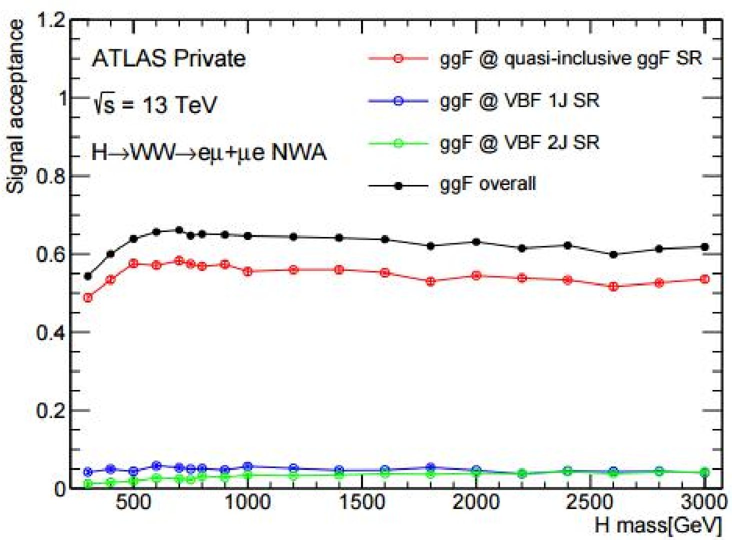

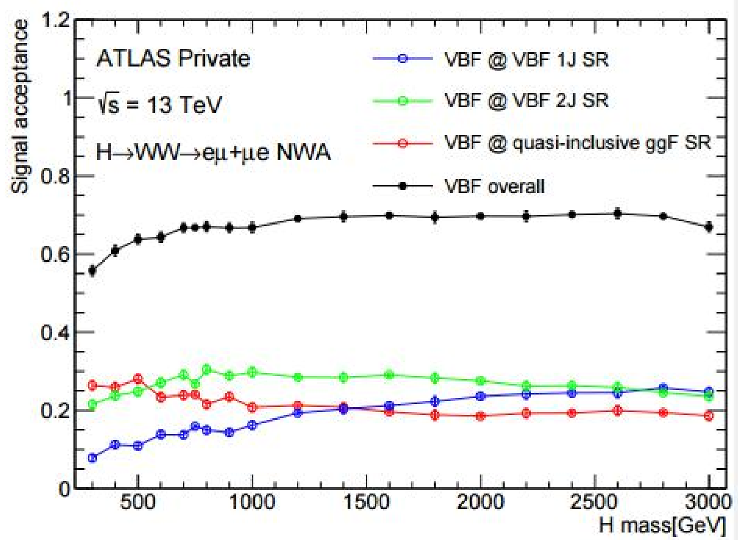

High-mass: CR event selections

- Event selection in control regions(CRs) :
  - VBF 1J phase space: $N_{\text{jet}} = 1:\ |\eta_j| > 2.4 \text{ and } \min(|\Delta\eta_{j\ell}|) > 1.75$
  - VBF 2J phase space: $N_{\text{jet}} \geq 2:\ m_{jj} > 500\text{ GeV and } |\Delta y_{jj}| > 4$

WW CR$_{\text{ggF}}$	Top CR$_{\text{ggF}}$	WW CR$_{\text{VBF1J}}$	Top CR$_{\text{VBF}}$
$N_{b\text{-jet}} = 0$	$N_{b\text{-jet}} = 1$	$N_{b\text{-jet}} = 0$	$N_{b\text{-jet}} \geq 1$
$\lvert\Delta\eta_{\ell\ell}\rvert > 1.8$	$\lvert\Delta\eta_{\ell\ell}\rvert < 1.8$	($\lvert\Delta\eta_{\ell\ell}\rvert > 1.8$ or	–
$m_{\ell\ell} > 55$ GeV		$m_{\ell\ell} < 55$ GeV)	–
$p_{\text{T}}^{\text{lead}} > 45$ GeV		$p_{\text{T}}^{\text{lead}} > 25$ GeV	$p_{\text{T}}^{\text{lead}} > 25$ GeV
$p_{\text{T}}^{\text{sublead}} > 30$ GeV		$p_{\text{T}}^{\text{sublead}} > 25$ GeV	$p_{\text{T}}^{\text{sublead}} > 15$ GeV
$\max(m_{\text{T}}^{W}) > 50$ GeV		–	–
Excluding VBF VBF1J and VBF2J		VBF1J phase space	VBF1J or VBF2J phase space

High-mass: top CR plots

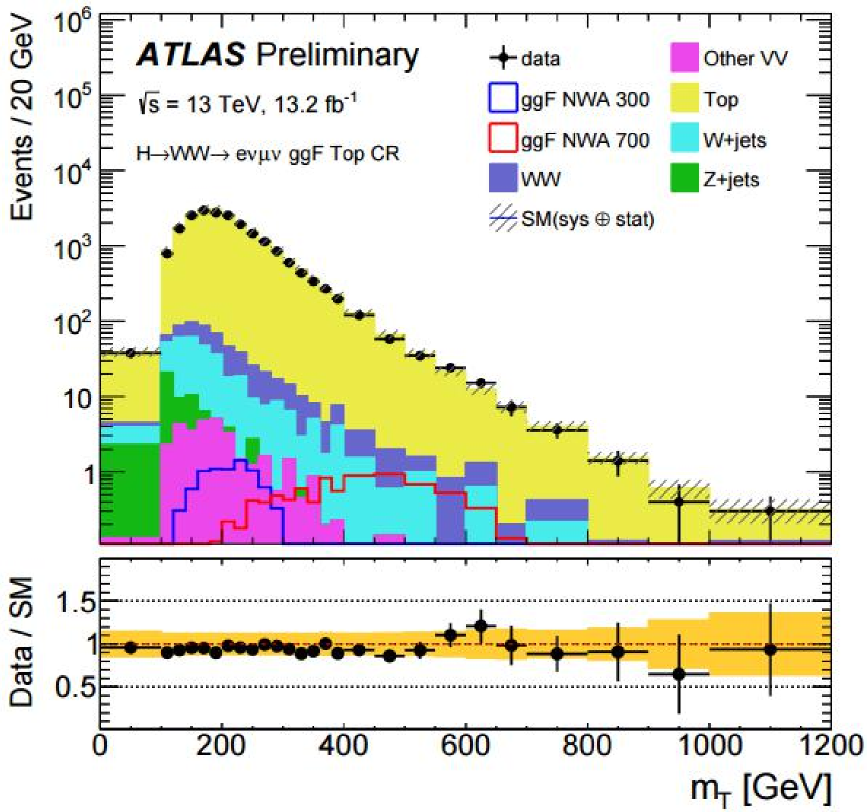

ggF Top CR

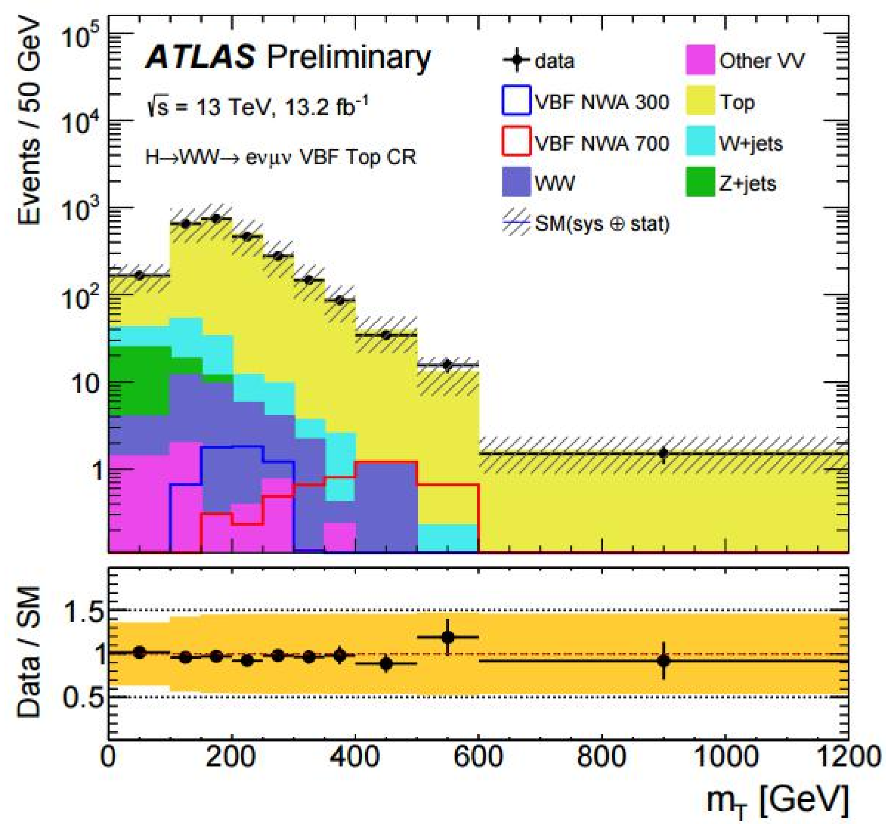

VBF Top CR

High-mass: WW CR plots

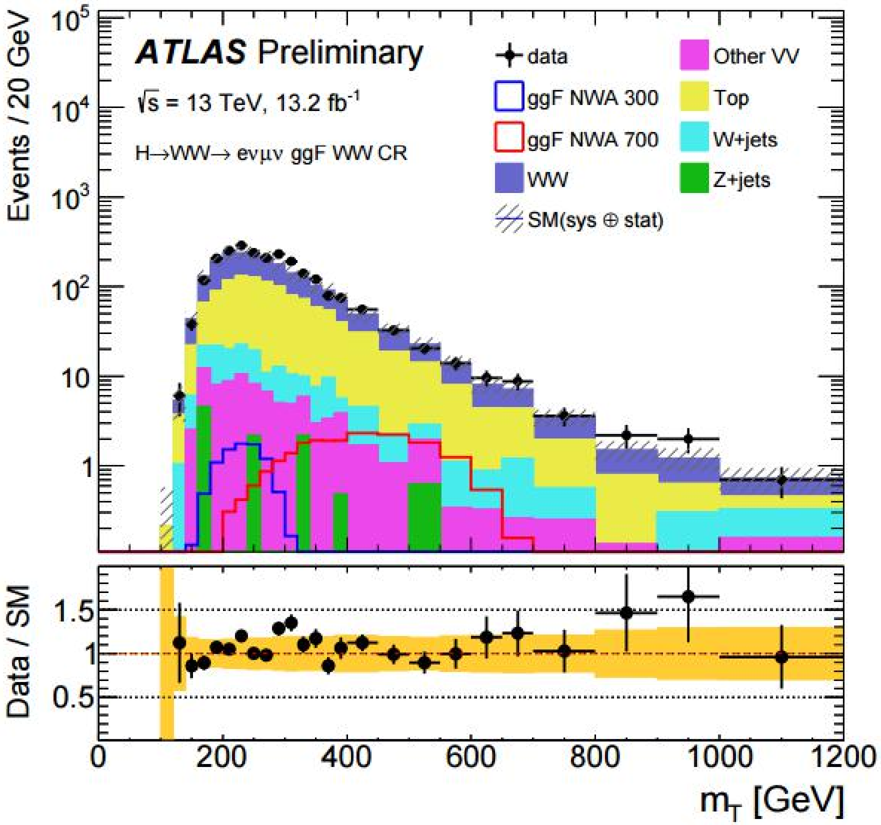

ggF WW CR

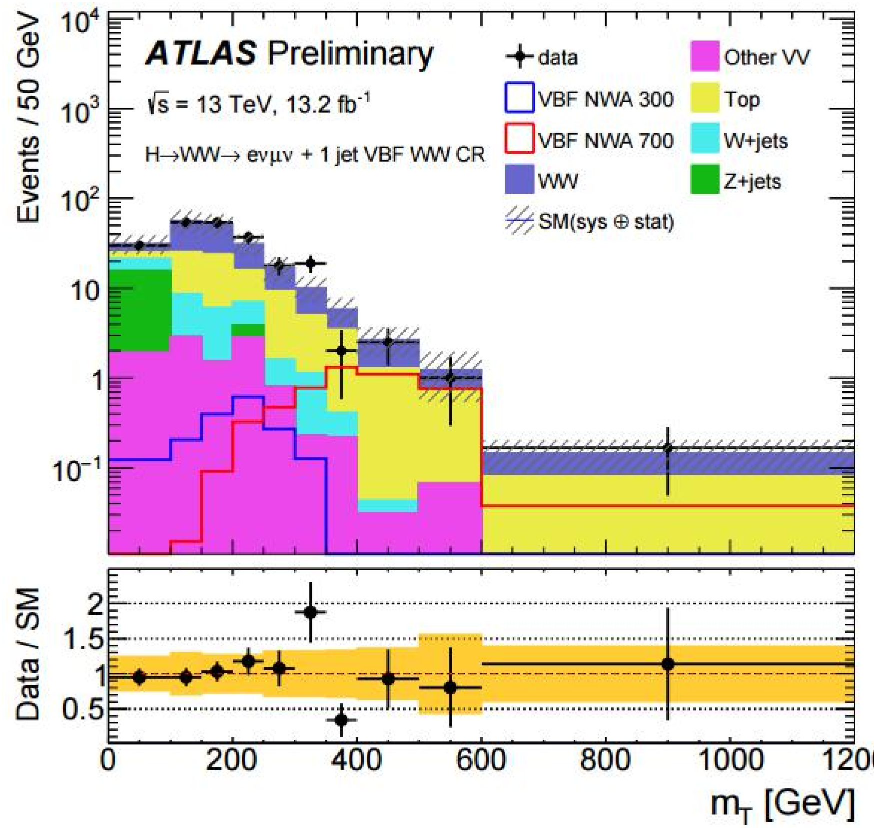

VBF WW 1J CR

High-mass: fake factor method

6.3 W+jets background

The background contribution is estimated using the fake-factor based data-driven method developed for the SM $H \to WW$ analysis [31] . The relevant information used for this analysis is shown here. The W+ jets background contribution is estimated using a sample of events satisfying all selection criteria but in which one of the two lepton candidates satisfies the identification and isolation criteria used to define the signal samples (these lepton candidates are denoted as "fully identified"), and the other lepton fails to meet these criteria and satisfies a less restrictive selection denoted as "anti-identified" (anti-id) lepton. From this data sample the non-W+ jets contribution based on MC predictions is subtracted. The purity of the samples is 55%, 64% and 38% for the quasi-inclusive ggF, $N_{\text{jet}} = 1$ and $N_{\text{jet}} \geq 2$ VBF categories, respectively.

The W+ jets contamination in the signal region is determined by scaling the number of events in the selected data sample by an extrapolation factor (fake-factor), which is measured in a data sample of di-jets events. The fake-factor is the ratio of the number of fully identified leptons to the number of anti-identified leptons, measured in bins of anti-identified lepton p_{T} and η. The systematic errors associated with the fake factor evaluation are described in Section 7.3.

High-mass: NFs and event yields

- Normalization factors(NFs)

$$NF^{Top}_{ggF\,CR} = 0.96^{+0.09}_{-0.08} \qquad NF^{Top}_{VBF\,CR} = 0.96^{+0.12}_{-0.14}$$

$$NF^{WW}_{ggF\,CR} = 1.3^{+0.1}_{-0.1} \qquad NF^{WW}_{VBF1J\,CR} = 1.2^{+0.5}_{-0.3}$$

- Event yields (statistical and systematic uncertainties combined)

	SR_{ggF}	Top CR_{ggF}	WW CR_{ggF}
WW	5300±400	430±90	1430±120
Top-quark	4200±400	20560±210	900±100
Z/γ^*	557±25	46±12	10.7±1.0
W+jets	450±120	260±80	105±30
VV	323±12	37±4	88.5±3.4
Backgrounds	10790±110	21330±180	2530±40
Data	10718	21333	2589

	SR_{VBF1J}	SR_{VBF2J}	Top CR_{VBF}	WW CR_{VBF1J}
WW	197±31	53±15	37±4	117±21
Top-quark	141±26	124±19	2650±80	65±14
Z/γ^*	20±7	12±4	40±17	27±5
W+jets	22±6	7.5±2.2	95±25	24±6
VV	9.5±1.0	5.7±0.8	5.2±2.2	11.0±1.5
Backgrounds	389±22	202±14	2830±70	247±16
Data	384	203	2825	253

High-mass: fitting procedure

- Likelihood function defined using MT distributions, as a product of Poisson functions over following 7 regions:
  - ggF SR: 26 bins
  - VBF 1J, 2J SRs: 10 bins
  - ggF Top, WW and VBF Top, WW 1J CRs: 1 bin
- Profiled likelihood method was used
- For the observed limits for ggF(VBF), VBF(ggF) cross section treated as a nuisance parameter, and profiled using a flat prior

High-mass: dominant systematics

- Main experimental uncertainties
  - Dominant Top uncertainties from jets: 9.8%, 12% for VBF1J, 2J SRs
  - Dominant WW uncertainties from jets: 16%, 23% for VBF1J, 2J SRs
- Main theoretical uncertainties on backgrounds
  - Dominant Top uncertainties from generator modelling: 17%, 48% in VBF 1J, 2J SRs. Also 35%, 48% for WW uncertainties
  - Similar in CRs, so the extrapolation uncertainties from CRs to SRs remain small
- Main theoretical uncertainties on signals
  - Dominant scale uncertainties on category migration: 30% increased to 90% from 300 GeV to 3 TeV for VBF 1J, 25% increased to 40% from 300 GeV to 3 TeV

High-mass: systematics (1)

- Total luminosity uncertainty: 2.9% (data15: 2.1%, data16: 3.7%)
- Main experimental uncertainties (in %):

	Top-quark			WW		
Source	SR_{ggF}	SR_{VB1J}	SR_{VBF2J}	SR_{ggF}	SR_{VBF1J}	SR_{VBF2J}
Jet	4.6	9.8	12	1.3	16	23
b-tag	17	6.2	13	1.7	0.99	3.3
MET	0.09	0.03	0.37	0.22	0.18	0.46
JVT	2.1	0.73	2.2	1.0	0.45	1.8
MC Stat.	0.42	2.4	2.5	0.58	2.7	4.8

- Top background theoretical uncertainties
  - Dominating uncertainties from ME: 17%, 48% for VBF 1J, 2J SRs
  - Similar in CRs, so the extrapolation uncertainties from CRs to SRs remain small

Error source
ME
PS
Radiation (radHi)
Radiation (radLo)
$Wt - t\bar{t}$ interference
Relative variation of σ_{st} (±20%)
PDF (down/up)

High-mass: systematics (2)

- WW background theoretical uncertainties
  - Dominating uncertainties from ME+PS: 35%, 48% for VBF 1J, 2J SRs
  - Extrapolation uncertainties still small

Error source
ME+PS
Renormalisation scale (0.5)
Renormalisation scale (2)
Factorisation scale (0.5)
Factorisation scale (2)
Qsf scale (0.5)
Qsf scale (2)
CKKW matching (down)
CKKW matching (up)
PDF (down/up)

  - NLO EW correction in the dominant qq→WW process was considered as normalization and shape uncertainty
  - Addtional k-factor of 1.7 as higher order correction in gg→(h*)→WW process with 60% uncertainty

- For both Top and WW, shape uncertainties also considered

High-mass: systematics (3)

- Dominating W+jets fake-factor estimation uncertainties
  - EW contribution: 15% for both e and μ in VBF 1J and 2J SR
  - Sample composition uncertainties, in ggF SR, VBF 1J and 2J SR respectively:
    - e: 26%, 21% and 21%
    - μ: 12%, 16% and 16%
  - Statistical uncertainty: < 1%
- Dominating signal theory uncertainties
  - Scale uncertainties on category migration
    - ggF: 10% over full mass range
    - VBF 1J: 30% increased to 90% from 300 GeV to 3 TeV
    - VBF 2J: 25% increased to 40% from 300 GeV to 3 TeV
  - Scale uncertainties on acceptance: relatively small
  - PS, underlying event and PDF uncertainties: relatively small
- For signal, we also have a correction on VBF due to PowHeg mismodelling

High-mass: top p_T^{lead} shape correction

- Mis-modelling found in ggF inclusive Top CR

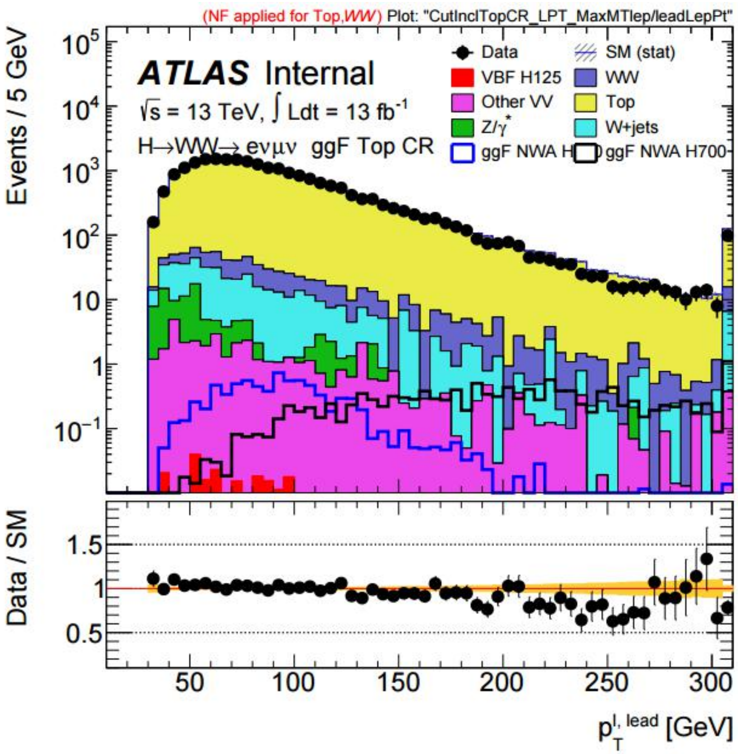

leading lepton p_T

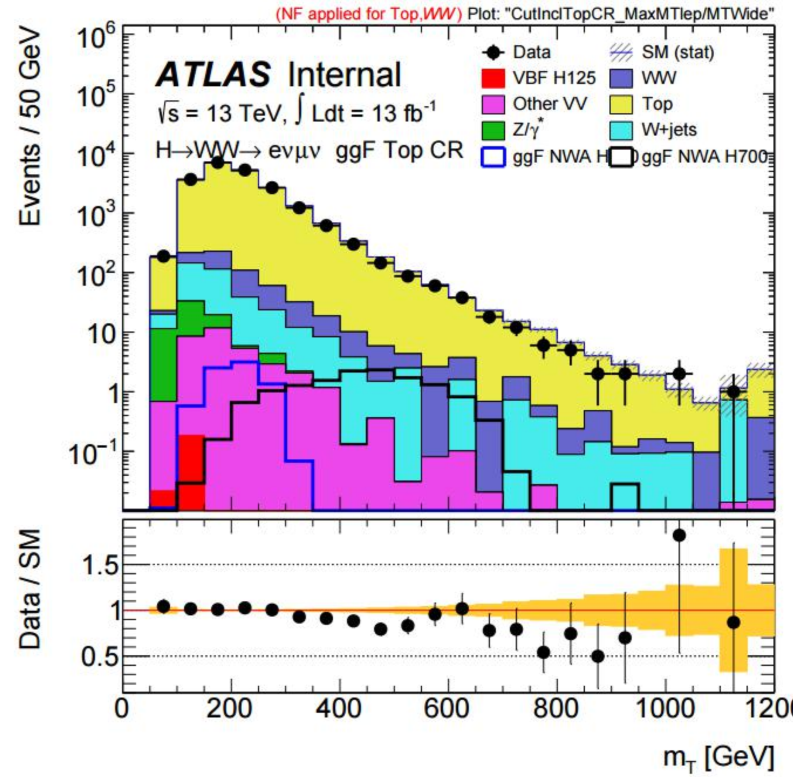

m_T

- This mis-modelling was less pronounced with DS1 data samples, and consistent with the NNLO QCD correction.
- No such mis-modelling observed in the VBF categories

High-mass: top p_T^{lead} shape correction

- The correction used a reweighting with linear fit function in ggF Top CR

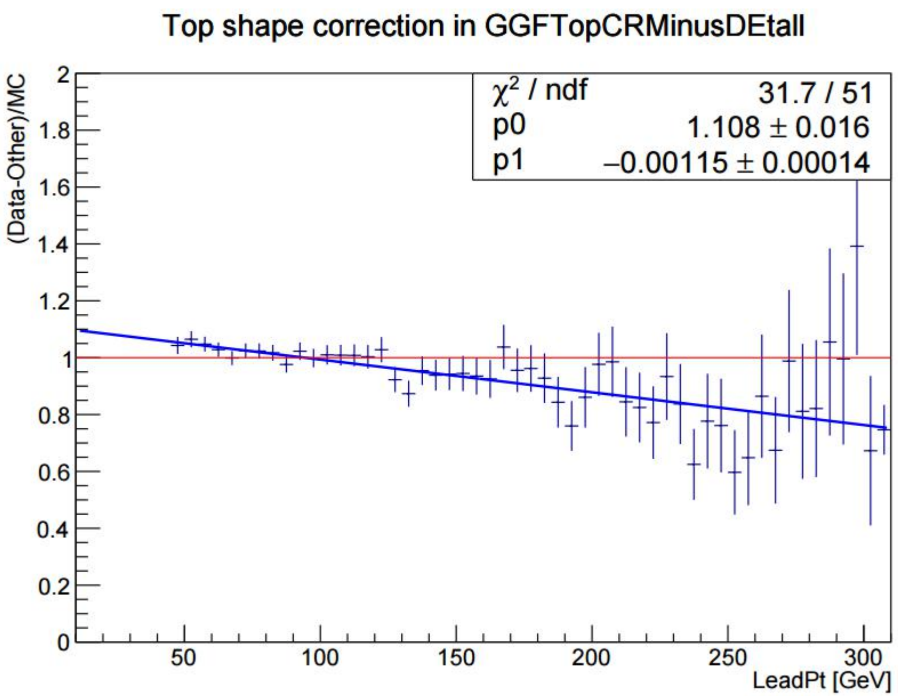

- ➢ No discrepency between em and me
- ➢ DEtall cut has no effect on the correction
- ➢ Applied to ggF SR, WW and Top CRs
- ➢ Shape uncertainties also considered